Large Eddy Simulation of confined, swirled jet

Master Thesis

By

Manasseh Anand Makhesh

CIMNE
Universitat Politecnica de Catalunya

A thesis submitted for the degree of
Master of Science in Computational Mechanics

Accomplished on
June 2013

Supervised by

Prof. Fabio Inzoli, Director – Deparment of Energy, Politecnico di Milano, Italy
Prof. Ramon Codina, CIMNE, UPC-BarcelonaTech, Spain

Abstract

Large Eddy Simulations (LES) of confined turbulent swirling flows in a swirl combustor are carried out. The simulations are based on a high-order finite difference method on a Cartesian grid, with the sub-grid scale stress tensor modeled using a scale-similarity model. The aim of this work is to study the physics of the flow and to evaluate the performance of LES method for simulation of the major features of turbulent swirling flows – the vortex breakdown, the highly anisotropic and fast-decaying turbulence structure. Influences of inflow/outflow conditions, combustor geometry, inlet swirl profile and turbulence structures are investigated.

Initially, a turbulent channel flow test case is used to verify and validate the implementation of LES in Fluent™ solver. Then for two different swirl numbers, the swirl combustor is modeled using Gambit and exported to Fluent for LES computations. This thesis work reports the results of numerical investigations of swirling turbulent jet flows by large-eddy simulation.

As the swirl number increases, the coherent structures become more evident and the internal recirculation zone moves upstream. LES successfully simulated the vortex breakdown, the internal recirculation zones and the anisotropic turbulence structures for all the swirl numbers considered. The resulting large-eddy simulation method is validated against the experimental LDV (Laser Doppler Velocimetry) and PIV (Particle Image Velocimetry) data of swirl combustor. The LES results are shown to be in good agreement with the experimental data if appropriate inflow and outflow boundary conditions are imposed.

Key words: swirling flow; large eddy simulation; internal recirculation zone; vortex breakdown; boundary conditions

Acknowledgements

Firstly I would like to thank my supervisor Prof. Fabio Inzoli at Politecnico di Milano who followed carefully the progression and quality of the work through a defined schedule and was always available for any assistance. Moreover I would like to express my sincere gratitude to Paolo Lampitella for his regular support regarding the implementation or technical problems. I appreciate the professional and friendly work atmosphere at "*CFDLab@Energy - Politecnico di Milano*" and also grateful for their computational resources.

Finally I thank my professors from UPC, Pedro Diez and my supervisor, Ramon Codina, to have allowed me to realize my master's thesis abroad during the double degree program, being always motivating and available for any advice.

Contents

Chapter 1

Introduction

There is an ever growing industrial demand for the numerical simulation of complex industrial flow problems. Although historically Reynolds-Averaged Navier-Stokes (RANS) methods have been widely used for such applications, there are many flow cases for which RANS simulations are not suitable. As the computational methods are now part of the everyday design practice, quality and reliability have become fundamental aspects even in relation to the numerical tools used in the design process. This is even more true in relation to the widely adopted commercial solvers because the user has a limited control on the computational tool. Hence it is necessary to deal with the verification that a certain computational tool has the prescribed accuracy in solving the underlying mathematical model and the validation of this mathematical model against the physical reality.

Turbulent flows are inherently unsteady, three-dimensional, and exhibit fluctuations over a wide range of spatial and temporal scales. For sufficiently high Reynolds numbers, energy is transferred from large to small scales, with the cascade process, at a rate which depends on the large scales only. The viscosity comes into play just to determine at which scales the viscous dissipation takes place. The large scales are anisotropic (i.e., they depend on the geometry of the flow), contain the most of the kinetic energy and completely determine the energy transfer rate to the smaller scales. The small scales are nearly isotropic, universal (i.e., similar among different flows) and much less energetic than the large ones.

With advancement in the computational power, simulation of turbulence has become feasible. RANS models have relatively low accuracy and limited to steady computations and they also have a low computational cost. There is a need to find more accurate turbulence modeling approaches. The LES approach is strongly connected to the numerical method adopted to solve the equations which, in turn, cannot be chosen independently from the filtering approach.

With the increased availability of computational resources, making a practical LES computation has become a real possibility. It is also connected to a greater accuracy and generality offered by the new theoretical advancements in the LES field.

1.1 Problem Definition and Thesis Outline

In swirling flows, large velocity gradients exist; the flow structure is highly anisotropic. Increasing the Reynolds number results in more and more scales being created as the viscous dissipation takes place on smaller and smaller scales. For high Reynolds number, there exists a range of scales which are smaller than the largest ones (such that can be considered isotropic) but still large compared to the smallest (dissipative) ones (such that can be considered unaffected by viscosity).Viscosity comes into play at the smallest (dissipative) scales, and the dissipation is in balance with the energy transfer rate from the larger, energetic scales.

It is worth mentioning that the preceding reasoning is valid only in a global statistical sense and is not valid at any point of time. At the same time, the reasoning is valid only locally and for high Reynolds number flows, in the sense that, the small scales just exhibit a local isotropy. According to the finite volume methodology, the Navier-Stokes equations, as well as any other conservation or balance law, are not discretized in the differential form but in their original integral form.

The original integral formulation of any balance law is actually a balance equation for a cell-averaged quantity; the most important thing, as recognized by Schumann [51] is that this quantity can be readily interpreted in the LES framework as a locally filtered variable.

Large eddy simulation (LES) provides an effective tool for handling complex turbulent flows. It has several advantages over those turbulence models within the Reynolds-averaged Navier-Stokes (RANS) framework. LES needs only to model small-scale eddies that are not supported by the spatial filter. Since the small eddies contain less turbulent kinetic energy, have a more universal behavior and are more isotropic, it is relatively easy to model them. LES can resolve all eddies in turbulence and becomes direct numerical simulation (DNS), if the grid resolution is high enough. Another important feature of LES is its ability of capturing the unsteady motion that may be important in turbulent swirling flows. Unsteady motion of coherent, non-turbulent structures can occur at high swirl numbers – which is known as the 'precessing vortex core (PVC)'.

LES required a time-dependent turbulent inflow condition since the simulated turbulent flow is time dependent. Similar to the inflow condition, outflow condition is also important for LES.

In this work, we examine the performance of LES for simulation of turbulent swirling flows in a swirl combustor configuration. The focus is on assessing the influence of the inflow and outflow boundary conditions as well as other geometrical and flow parameters on swirling flow simulations. The first part of this thesis is to investigate the quality and reliability of the LES module implemented in the widely used commercial CFD solver Fluent. More specifically, it is aimed at determining the influence of all the relevant numerical parameters in an LES computation and identify the correct LES approach with the Fluent solver. Then the next part is to apply the investigations to the swirling jet problem whose experimental data LDV and PIV are known.

Finally the numerical results obtained are compared with the available experimental data and the accuracy of LES computation is shown. The influence of these conditions on the mean flow field and the turbulent kinetic energy distributions are explored.

1.2 Why LES?

As discussed in the previous paragraph, there are several methods currently available to deal with the scale separation problem in the numerical simulation of turbulent flows that is the difference between the smallest and the biggest active scale in the flow, which increases with the Reynolds number. Despite their similar nature (i.e., all of them rely on a reduction of the number of scales to be resolved), they have important conceptual differences which need to be highlighted to understand their applicability.

A first important difference is the number of physical scales resolved, which ranges from zero in the RANS approach to all the scales up to the smallest flow dependent one in the LES approach, with the URANS approach resolving just few non turbulence-related scales. Aside from the obvious practical implications, like the cost of the simulation (in terms of the total number of operations required to obtain a solution in a given domain) and the amount of information provided by it, what is equally important is the physical relevance of the underlying approximation. The former aspects are probably the two most influential factors in any practical CFD application in industry; the latter is mostly related to the quality and reliability of the results of the simulation which, in turn, still have an effect on the cost of the simulation (in terms of the effort, monetary or not, required to deal with the confidence in the results).

The physical aspect essentially regards the connection between the scales which are relevant in the simulation of the flow problem and the range of scales which are effectively resolved. In practice, the issue is which scales (and in what amount with respect to their totality) are modeled, instead of correctly represented, and what is the influence of this choice. This introduces a clear distinction between the correct ranges of applicability of a modeling approach and the cases for which its results are reliable.

The RANS/URANS turbulence models are, by definition, designed to take into account all the turbulent scales, mostly the geometry dependent ones. However, they still rely on a sort of reverse engineering in which the scale dependency of the model is tuned to perform well in selected applications. While this is in full agreement with the engineering approach (i.e., the use of a model to reduce the costs of a simulation) and some of these models can correctly model several large scale features of different kind of flows, there are cases in which they simply do not perform well.

Typical examples are the free shear flows, ranging from mixing layers to the wakes of bluff body flows and turbulent jets, in which the mean flow properties are influenced by most of the modeled turbulent scales. This is even more true when qualitatively and quantitatively different turbulent scales interact in the same flow problem, as the behavior of the models is practically unpredictable. Nonetheless, the use of a

RANS/URANS approach is correct in these cases too and the current industrial practice is essentially based on the use of application-specific in-house modifications to the models

1.3 Experimental Methods LDV and PIV

Laser Doppler Velocimetry (LDV), also known as laser Doppler anemometry (LDA) is the technique of using the Doppler shift in a laser beam to measure the velocity in transparent or semi-transparent fluid flows. It is often chosen over other forms of flow measurement because the equipment can be outside of the flow being measured and therefore has no effect on the flow.

Particle Image Velocimetry (PIV) is an optical method of flow visualization. It is used to obtain instantaneous velocity in fluids. The fluid is seeded with tracer particles which, for sufficiently small particles, are assumed to faithfully follow the flow dynamics. The fluid with entrained particles is illuminated so that particles are visible. The motion of the seeding particles is used to calculate velocity field of the flow.

For swirling flows at high Reynolds numbers, different patterns of coherent structures have been documented by advanced experimental methods LDV and PIV at different conditions. The scope of this thesis is to obtain the LES numerical results for the swirl combustor and compare with the available experimental data.

Chapter 2

Large Eddy Simulation of incompressible flows

2.1 The LES framework

As in all the turbulence modeling approaches, the starting point in LES are the governing equations of the fluid flow. In the case of incompressible isothermal flow of a Newtonian fluid, the Navier-Stokes equations can be usefully rewritten in the following differential divergence form:

$$\frac{\partial u}{\partial t} + \nabla \cdot F(u) = 0$$

$$F(u) = uu + p/\rho_0\, I - 2\nu\nabla^s u$$

$$\nabla \cdot u = 0$$

Where I is the identity matrix, ∇^s is the symmetric part of the gradient, u is the three-dimensional velocity field, p is the pressure, $\rho_0$is the constant density (from now on absorbed in the pressure) and ν is the kinematic viscosity. As the LES approach is essentially based on the resolution of the large scales only, it is possible to define the following formal decomposition of the velocity field.

$$u(x,t) = \bar{u}(x,t;\overline{\Delta}) + u'\left(x,t;\overline{\Delta}\right)$$

Where $\bar{u}$ is the large scale part of the velocity field and u' represents the small scale part. In general, both the large and the small scale fields in LES are three-dimensional and unsteady. Moreover, the parameter $\overline{\Delta}$ is introduced, which specifies the smallest length scale correctly represented by the velocity field $\bar{u}$.

The error committed on the specific statistic Q (available from the experimental data) applied to the numerical solution u^dcan be formally decomposed into scale separation error, projection error, numerical error and modeling error.

2.2 Boundary Conditions in LES

The discussion so far regarded the general LES framework and the modeling of the SGS tensor. However, in order to obtain a well-posed problem, the LES equations require the setting of appropriate initial and boundary conditions. This is a very complex aspect of the LES, on the theoretical as well as on the practical side, and cannot be exhausted in a few

pages; as a consequence the discussion will keep general and only the main issues will be presented.

Generally speaking, two main questions arise when dealing with the definition of boundary conditions in LES: what kind of boundary conditions are required for the filtered variables and what is the amount of information required at boundaries to properly represent a particular solution. In practice, this has to do with inflow and wall boundary conditions while the outflow boundary condition, even if relevant, is not specific of the LES and will not be considered [52].

The first question arises because the filtered and the unfiltered velocity field are not governed by the same set of equations; indeed, filtering on a bounded domain will usually produce a commutation error which explicitly depends on the unfiltered velocity field and should be modeled. In addition to this, where the commutation error is not present, the inclusion of a SGS model can alter the original degree of the equations by the introduction of higher-order derivatives; this in turn prevents that the original form of boundary conditions for the Navier-Stokes equations can be used to obtain a well posed problem. However, even if this problem is still open, it is not usually considered arguing that the higher-order derivatives are also higher-order perturbations of the Navier-Stokes equations and the same boundary conditions can be used [53].

Instead, the answer to the second question is quite straight and cannot be circumvented: the amount of information required at boundaries and as initial condition is directly proportional to the number of degrees of freedom represented at the boundaries and in the domain respectively. Roughly speaking, if an inflow boundary has been discretized with a grid and time step which can represent up to certain length and time scales then the solution at these scales must be assigned and the same is true for an initial condition in the interior of the domain.

Assigning these conditions on the basis of mean quantities only amounts to arbitrarily set to zero the energy content in most of the resolved part of the spectrum and, as a consequence, to arbitrarily pick one of the infinite possible solutions. This has a high influence on the reliability of the LES results as experience shows that limiting the information to mean flow quantities is not sufficient and usually produces completely erroneous results, even for the mean flow quantities. Even when these conditions are assigned there are still some open issues concerning the reliability of the results. Indeed, even if the true LES boundary conditions were known, they would still differ from the unfiltered velocity field because of the action of the scale separation operators acting on it (mostly the grid). This, in turn means that infinite unfiltered velocity fields could still be associated with these boundary conditions and because of the non-linearity, the missing scales would interact differently with the resolved ones giving rise to different resolved velocity field. This issue, which is not limited to the boundary conditions but regards the LES approach as a whole, is complementary to that introduced before because different best solutions (which differ by the definition of the unavoidable associated error) differently interact with the presumed sub-grid scales giving rise, again, to different resolved velocity field. As a matter of fact, the interior of the domain as well as on the

boundaries, the LES approach always assumes that the missing scales are locally isotropic, dissipative and have a universal character.

In practice, the velocity field at inflow boundaries, as well as in the interior domain at the initial time, is never known up to the cutoff length scale and the only way to set meaningful boundary and initial conditions is to approximately reconstruct it by adopting the following decomposition:

$$\overline{u}(x,t) = \overline{U}(x,t) + \overline{u'}(x,t)$$

Where $\overline{U}(x,t)$ is the mean-flow part, usually known by experiments, by URANS computations or in analytical form, and $\overline{u'}(x,t)$ is a fluctuation which can be generically written as:

$$\overline{u'}(x,t) = \sum_{n=1}^{N} [a_n \cos(k_n \cdot x + \omega_n t) + b_n \sin(k_n \cdot x + \omega_n t)]$$

Where N is the number of Fourier modes assigned, a_n and b_n are the amplitudes corresponding to the wave vector k_n and ω_n are time frequencies.

What explicitly differs between the assignment of inflow boundary conditions and the initial conditions is just the time dependency and the definition of the time frequencies. In contrast to a choice of assigning a distribution of the form $\omega_n = f(k_n)$, the initial condition is defined by a steady mean flow part and $\omega_n = 0$.

However, several situations exist in which the time evolution of the flow is not of interest and the main issue is to reach the statistically steady state as soon as possible.

The boundary conditions at walls also require attention because the flow dynamics in the near-wall region of boundary layers is very different from the ideal isotropic turbulence case. Indeed, the flow driving mechanism (i.e., those responsible for the turbulent kinetic energy production) are mainly associated to length scales which depends on the Reynolds number, are strongly anisotropic and connected to the backward energy cascade which is largely dominant over the forward cascade in certain regions of the boundary layer. This has two main consequences: an LES approach is no more formally valid if the scales associated to the flow driving mechanisms are not properly resolved and the usual SGS models are totally inadequate to represent the missing scales. In addition, in the region very near to the wall (viscous sub-layer), the flow is not even turbulent and the SGS model adopted is required to recognize this local behavior and adapt to it. To circumvent these issues there are two possible approaches:

Direct resolution of the near-wall flow dynamics: It simply consists of using a sufficiently fine resolution to capture the flow-driving mechanisms, adopting a SGS model capable of modifying its local behavior according to the local flow characteristics and setting the classical no-slip boundary conditions at walls. In practice, this requires a DNS-like resolution in the near-wall region but because of the wall, the smallest dynamically active

length scale is now dependent on the distance from the wall and the computational cost is somewhat higher than the requirement.

Modeling the near-wall flow dynamics: An alternative to the previous approach, which becomes unfeasible for high Reynolds numbers, is to model the near-wall region instead of resolving it. In practice, since the distance from the first grid-point to the wall (as well as the grid spacing in the two other directions) is greater than the minimum characteristic length scale of the region, it consists in substituting the no-slip boundary condition at the wall with a model-dependent boundary conditions. The models of this class, also known as wall models, are clearly different from the SGS models introduced previously because they have to represent scales which are not simply dissipative but are the driving mechanism in the region; in this sense, these models can be interpreted as RANS models because they have the same goal.

Chapter 3

Finite volume solver: Fluent™

3.1 Numerical Schemes suited for LES

The CFD solver Fluent employs a cell-centered, co-located finite volume discretization of the governing equations. To prevent the non-monotone behavior of the pure central scheme, a bounded central scheme is available in the solver. It is based on the Normalized Variable Diagram and the Convection Boundedness Criterion. The discretization of the diffusion term in a finite volume method requires the computation of the gradient at face centers starting from its values in the cell centers. The final step to obtain a computable model is the discretization of the time derivative term. Among the different methods available in Fluent, the only one which is suitable for the LES approach is the second-order backward differencing scheme. Among the several methods available in the solver to deal with the pressure-velocity coupling issue, the fractional-step method is the one best suited for LES computations.

3.2 Accuracy Assessment

As a first step in the evaluation of the code capabilities for LES computations, it is mandatory to assess the accuracy of the solver and to verify under which conditions its theoretical accuracy is obtained. The leading term in the discretization error for the generic component of the velocity field at the time $t = n\Delta t$ on a Cartesian grid with uniform spacing $\Delta x = \Delta y = h$ is proportional to [54]:

$$\|U^n - u(n\Delta t)\| \propto n\Delta t(\Delta t^2 + h^2)$$

Where the h^2 term accounts for the spatial discretization error and the Δt^2 term accounts for the time discretization error and the error committed in the approximate factorization of the fractional step.

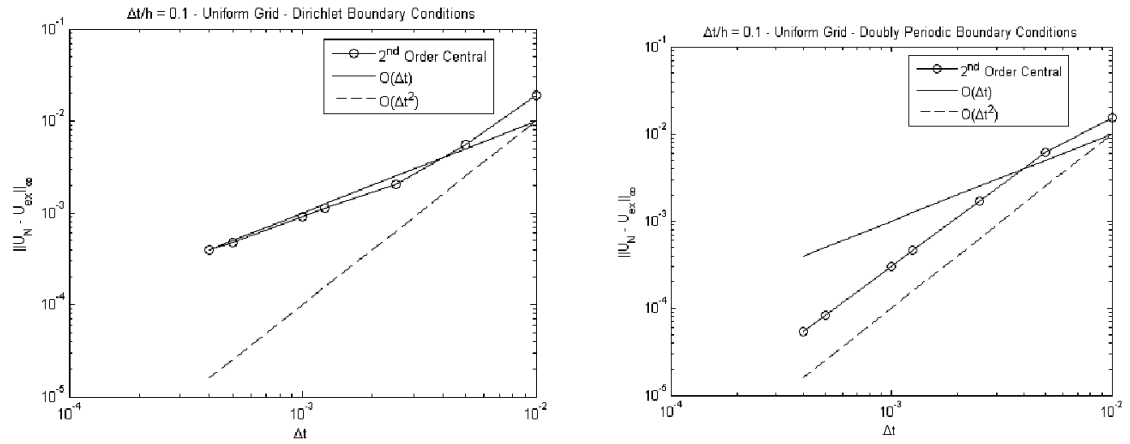

Figure 2.1: Effect of the boundary conditions on the discretization error for a uniform Cartesian grid.

Hence the error is expected to decrease as the second power of the time step. This is confirmed in the case of periodic boundary conditions but not for Dirichlet boundary conditions, which influence the solution with a first order error term proportional to $(h/\Delta t)\Delta t$. As clearly seen, the error first decreases with the second power of the time step and then, for lower values of the time step, its accuracy is reduced to first order only; this is clearly identifiable as a boundary condition effect, since all the other settings have been kept equal in both the computations. The time step in LES should be limited to avoid the additional filtering effect of the time discretization error, which is usually considered negligible.

3.3 LES implementation in Fluent™

It is mandatory to describe the specific approach adopted in the solver and how it is effectively implemented. The first aspect to note is that, being based on the finite volume method, the Fluent™ solver is by itself based on the explicit approach with $\overline{\Delta} = h$. The integral form of the Navier-Stokes equations is actually a balance equation for a top-hat filtered variable:

$$\frac{1}{|V(x)|}\int_V U\ dV = \frac{1}{\Delta^{-3}(x)}\int_V U\ dV = \overline{U} = G * U$$

where, in the specific case of the finite volume method, $|V(x)|$ is the volume of the generic integration cell. The full equivalence of the numerical method employed in the solver can be recognized by analyzing the approximation adopted in the surface integrals:

$$G * [\nabla \cdot (\blacksquare)] = \frac{1}{|V(x)|}\int_V \nabla \cdot (\blacksquare)\, dV = \frac{1}{|V(x)|}\int_{\partial V} \mathrm{n} \cdot (\blacksquare)\, dS$$

$$\cong \sum_{f=1}^{N_f} (\blacksquare)_f \cdot n_f \frac{|A|_f}{|V|} = G^d * [\nabla^d \cdot (\blacksquare)]$$

which shows that all the discretized spatial terms explicitly contains the numerical filter G^d whose approximation is due to the fact that the sum involves only the values at the center of the faces.

Moving on to the SGS models, Dynamic Smagorinsky model is the one which deserves more attention. When derived in the finite volume framework, the actual form of the dynamic constant is different from the original one. In particular, the finite volume form does not require any commutation property, which is consistent with the finite volume LES approach.

Chapter 4

Numerical investigations of turbulent channel flow

4.1 Introduction

The LES approach to the turbulence modeling and the finite volume solver Fluent were discussed in the previous chapters. The main drawback emerging from these discussions is that (as in most of the current applications with the majority of CFD solvers) the LES methodology implemented in Fluent is strongly influenced by the numerical method as it is not based on the explicit filtering procedure.

It follows that the quality and reliability of the results provided by the solver with the LES approach are strongly connected to the numerical procedures adopted. The three main issues are as follows:

- *Definition of a proper grid*: as the filter is defined as a cell-centered top-hat (local volume average) with cutoff length $\overline{\Delta}= \sqrt[3]{|V(x)|}$ (where $|V(x)|$ is the volume of the grid cell), the actual nominal filter is fully determined by the numerical grid adopted. This means that, to have a correct LES simulation, the grid has to follow the condition $\sqrt[3]{|V(x)|} < \ell_{EI}$. In practice, especially for complex applications, ℓ_{EI} is never known and can only be roughly estimated. This issue makes LES incomplete but, while this is common to all the LES approaches, when $\overline{\Delta}= \sqrt[3]{|V(x)|}$ there is no such thing as the grid convergence to ensure that the scales down to $\overline{\Delta}$ are correctly resolved.

- *Selection of a proper convective scheme:* It can be stated that not all the scales down to $\overline{\Delta}$ can be correctly resolved when $\overline{\Delta}= \sqrt[3]{|V(x)|}$. This is due to the truncation error of the convective scheme, which acts on the smallest resolved scales and is totally unaffected by the filtering. As a result, it is important to introduce the term "nominal resolution" to highlight that the range of correctly resolved scales is difference from the presumed one. There is no way to previously estimate it. Hence the selection of the convective scheme becomes essential in the determination of this range and obviously affects the definition of a proper LES grid. Two schemes available in Fluent are suitable for LES computations but as will be shown in this chapter, they also have very different behaviors.

- *Selection of a proper time step:* In the previous chapters, time discretization error was considered to be negligibly small but, in practice, this cannot be automatically assumed to be the case and hence has to be achieved by the selection of a proper time step. Moreover, the time step also influences the splitting error introduced by the fractional step method. It can be shown that, analogously to the spatial discretization error, the time discretization error can be interpreted (always together with the gird) as an additional scale separation operator. Hence the time step should be small enough compared to the characteristic time scales of the resolved flow.

The focus is on the determination of optimal numerical/modeling settings. Turbulent channel flow test case, for which several DNS databases at different Reynolds numbers exists is considered. This is a classical LES test case as it contains most of the physics present in practical applications while still preserving a very simple geometrical setting. As such it is very useful in determining the numerical dependencies with only minor efforts.

It has been clearly explained before that none of the LES approaches can lead to an error free computation of a generic statistic of the flow (i.e. $e^Q(u,u^d) \neq 0$), unless there is some fortuitous mutual error cancellation. For the specific approach used in fluent this means that, in the ideal case, there will always be the projection errors $e_N^Q(u,u^d)$ due to the grid and in general this error will also be accompanied by the modeling and numerical errors. In theory, to make a proper confrontation of the results with a reference DNS or with the experimental data, it would be necessary to apply the same scale separation operator to the reference data before applying any statistic. However, this is practically impossible (especially for the experimental data) as these are almost already available as statistics. There is no way to remove the projection error (i.e. the scale separation error associated to the grid) from the numerical solution. As a result, while not being strictly correct, in the vast majority of cases, the LES results are simply compared with the reference data without additional treatment and this approach has been followed in this thesis too.

4.2 Turbulent Channel flow test case

The case considered [42] is represented by the fully developed turbulent incompressible isothermal flow between two infinitely extended parallel flat plates separated by a distance $2H$. The mean flow direction is along the x axis, the wall normal direction is represented by the y axis and the z axis represents the span-wise direction, as depicted in figure (4.1). The velocities in the three coordinate directions are u, v and w respectively. The flow is statistically steady, homogeneous in the wall parallel directions and its statistics are dependent on the coordinate y only. Moreover, the plane $y = H$ is a symmetry plane for all the statistics.

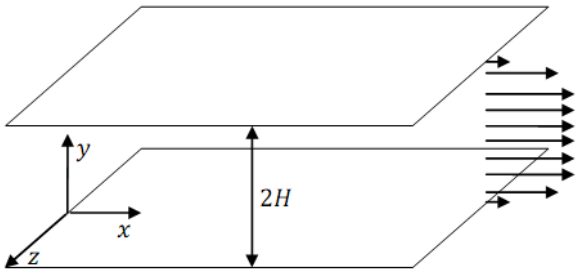

Figure 4.1: Sketch of the channel flow

The velocity field can be decomposed into an average part plus a fluctuation. By considering the no-slip boundary condition at walls and the divergence-free constraint, under the mentioned hypotheses, the turbulent channel flow is governed by the following form of the averaged Navier-Stokes equations:

$$\frac{\partial\langle p\rangle}{\partial x} = \frac{\partial}{\partial y}\left(\rho_o \nu \frac{\partial\langle u\rangle}{\partial y} - \rho_0\langle u'v'\rangle\right)$$

$$\frac{\partial\langle p\rangle}{\partial y} = \frac{\partial}{\partial y}(-\rho_0\langle v'v'\rangle) \qquad (4.1)$$

$$\frac{\partial\langle p\rangle}{\partial z} = \frac{\partial}{\partial y}(-\rho_0\langle v'w'\rangle)$$

where $\rho_0$is the constant density, ν is the kinematic viscosity and $\langle p\rangle$ is the average pressure field. The mean stream-wise pressure gradient depends on the axial coordinate only. As the Reynolds stress vanished at solid walls, it is evident that the viscous stress dominates close to the walls hence it is plausible that the viscosity ν and the wall shear stress τ_w are important parameters for this region.

4.2.1 General Computational details

Firstly, as the flow is homogeneous in the stream-wise and span-wise directions, all the numerical computations have been performed in a computational box of extension $L_x \times 2H \times L_z$ with periodic boundary conditions along x and z directions and no-slip conditions at the walls. It is worth mentioning that, since all the computations performed are inherently unsteady, this specific setting is not equivalent to the classical Eulerian frame but consists in following the same box of fluid as it evolves in time along the channel. At some time after an initial transient to be eventually disregarded (whose extent depends on the specific initial condition), the flow will be fully developed and statistically steady. The way this initial transient time is evaluated, and the necessary extension of the domain in the wall parallel directions to make the periodic boundary conditions a proper choice, will be both discussed later. Then, as the periodic boundary condition requires fixing of the mean axial pressure gradient to drive the flow, the following parameters have been fixed.

$$\rho_0 = 1\left[\frac{Kg}{m^3}\right]$$

$$\mu = \rho_0 \nu = \frac{1}{Re_\tau}\left[\frac{Kg}{m \cdot s}\right] \tag{4.2}$$

$$H = 1[m]$$

where the viscosity is set to be equal to the inverse of the Reynolds number. In this way the required pressure gradient and the friction velocity become independent from all the flow parameters.

Hence the dimensional equations that are solved can be considered similar to the equations non-dimensionalized by H and u_τ and the friction Reynolds number of the simulation can be changed by simply acting on μ. Also, the time in the simulations corresponds to a non-dimensional time $T = tu_\tau/H$ usually referred to as *Time Unit*. In all the computations the computational box is discretized by $N_x \times N_y \times N_z$ cells which are uniformly spaced in the homogeneous directions and non uniformly spaced in the wall normal direction, as depicted in figure (4.2).

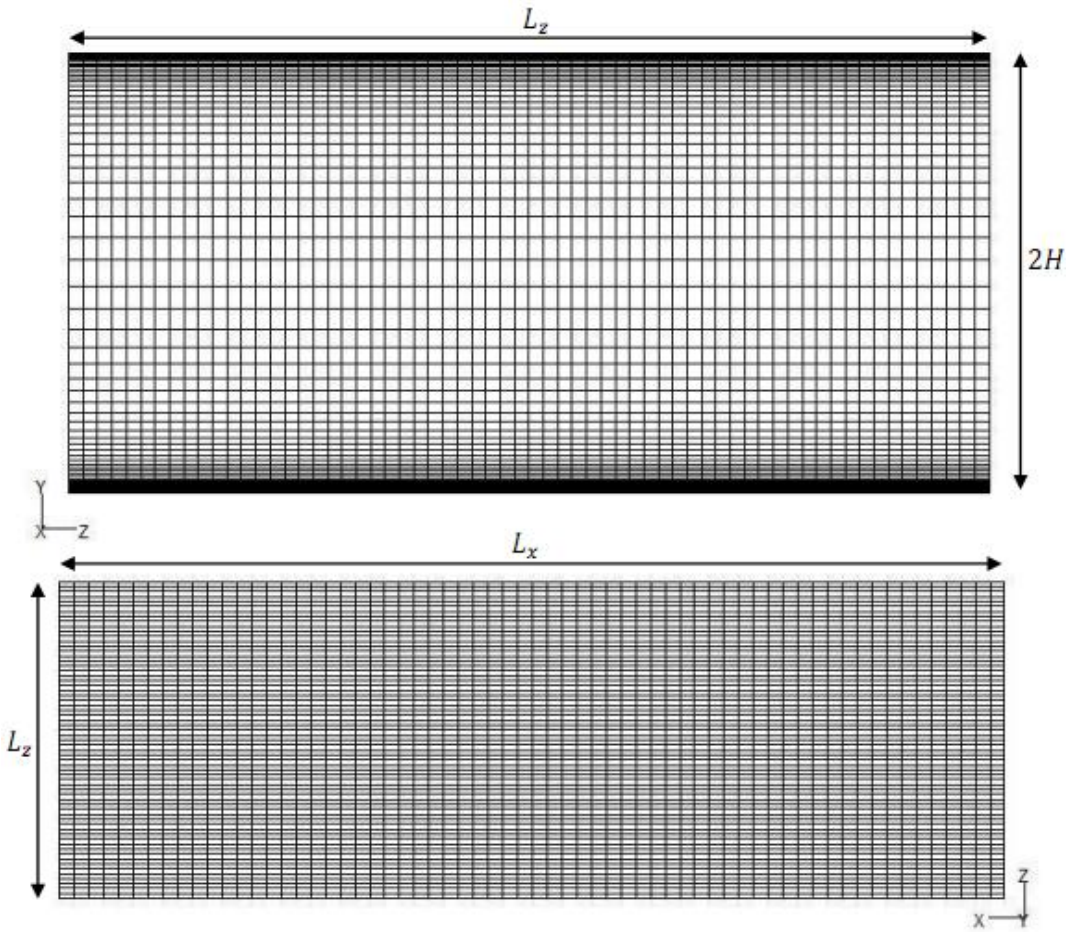

Figure 4.2: Sketches of a typical grid used in the channel flow computations

Finally it is important to explain how the computations are effectively carried out and how the numerical results are analyzed. In all the computations, an initial velocity field is assigned (how this is done will be specified case by case) and the computation is advanced in time until the statistically steady state is reached. This steady condition is usually considered to be reached when the computed total shear stress effectively becomes linear or alternatively when the wall boundary condition equation is shown to be satisfied by the numerical results. However, apart from some theoretical considerations, this check is also not easy to perform in a commercial CFD software as it requires the real time computation of several average quantities, which is not practical(at least for the initial transient time which will be finally disregarded). As a result, in all the present computations the steady state condition has been determined by monitoring the time evolution of the volume averaged (over the whole domain) resolved kinetic energy, as clarified in figure (4.3).

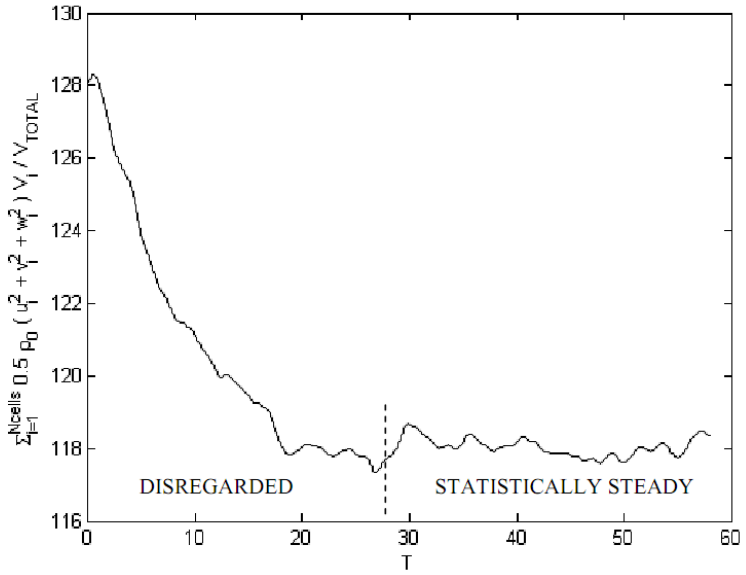

Figure 4.3: Evaluation of the steady state by the evolution in time of the volume averaged kinetic energy.

Once the steady state is reached, the solution has to be advanced in time and sampled until the necessary number of samples for the statistics is reached. In theory, the necessary number of samples should be determined, case by case, by monitoring how the statistics vary with this number and selecting the number for which they are no longer varying (at least not significantly). As the objective of the computations is to compare the numerical results for different numerical settings, in all the cases 60 samples have been considered for the statistics as this value has shown to be sufficient for all of them. The time separation between the samples will generally vary from case to case (as it is dependent on the time step adopted) and will be specified later.

For the channel flow test case, three kinds of results are of main interest. The mean velocity profile:

$$u^+ = \frac{\langle u \rangle}{u_\tau}$$

The r.m.s velocity fluctuations of the generic velocity component u_i:

$$RMS_{u_i} = \sqrt{\frac{\langle (u_i - \langle u_i \rangle)^2 \rangle}{u_\tau^2}}$$

and the discrete energy spectrum functions of the three velocity components in the two homogeneous directions. In selected cases these values will also be provided for the SGS viscosity ν_{SGS} as its behavior can be useful to clarify some aspects.

The samples for the ensemble averages in time are collected over a period $T_s = (N_s - 1)m\Delta t$, which will be specified case by case. In practice, the parameter m has been adjusted from case to case to obtain values of T_s which are as close as possible among all the computations.

Before introducing the numerical results for all the different settings analyzed, it is important to provide a summary of all the computations performed as shown in Table 4.1, wherein several physical and numerical parameters employed are reported. Apart from the several parameters already presented, the convective scheme (C.S.) and the SGS model (SGS) used for the simulations are also specified in the table. The halved value $\Delta y^+_{min}/2$ has been reported, as the value of interest for the cells at walls is the distance of the cell center from the wall. Moreover, to simplify the subsequent references to a specific computation, the cases have been numbered.

It can be seen that the major part of the computations have been performed for $Re_\tau = 180$, while only two simulations have been performed for $Re_\tau = 2000$. In practice, due to the big amount of computational resources required to perform the simulations at such a Reynolds number (the greatest one for which DNS data are currently available), these two simulations have been performed by adopting the wall function approach available in Fluent and they are the only ones in which the wall normal spacing is uniform. All the computations for the smaller Reynolds number have been performed with the wall-resolving approach.

Nº	Re_τ	L_x	L_z	$N_x \times N_y \times N_z$	Δx^+	Δz^+	$\Delta y^+_{min}/2$	Δt^+	C.S	SGS
1	180	$4\pi H$	$4\pi H/3$	128x129x128	17.67	5.89	0.13	0.045	C	N
2	180	$4\pi H$	$4\pi H/3$	48x129x48	47.12	15.71	0.13	0.27	C	N
3	180	$4\pi H$	$4\pi H/3$	48x129x48	47.12	15.71	0.13	0.27	C	DS
4	180	$4\pi H$	$4\pi H/3$	64x65x64	35.34	11.78	0.28	0.90	C	N
5	180	$4\pi H$	$4\pi H/3$	64x65x64	35.34	11.78	0.28	0.90	C	DS
6	180	$4\pi H$	$4\pi H/3$	64x65x64	35.34	11.78	0.28	0.90	BC	DS
7	180	$4\pi H$	$4\pi H/3$	64x65x64	35.34	11.78	0.28	0.27	C	N
8	180	$4\pi H$	$4\pi H/3$	64x65x64	35.34	11.78	0.28	0.27	C	DS
9	180	$4\pi H$	$4\pi H/3$	64x65x64	35.34	11.78	0.28	0.27	C	TKE
10	180	$4\pi H$	$4\pi H/3$	64x65x64	35.34	11.78	0.28	0.27	BC	N
11	180	$4\pi H$	$4\pi H/3$	64x65x64	35.34	11.78	0.28	0.27	BC	DS
12	2000	$2\pi H$	πH	64x65x64	35.34	98.17	30.77	0.30	C	DS
13	2000	$2\pi H$	πH	64x65x64	35.34	98.17	30.77	0.30	BC	DS

Table 4.1: Summary of the simulations performed for the turbulent channel flow test case. Legend – Convective Schemes (C.S.): C, Central Scheme – BC, Bounded Central Scheme. SGS Models (SGS): N, none – DS, Dynamic Smagorinsky Model – TKE, Dynamic model with a transport equation for the SGS Turbulent Kinetic Energy.

4.2.2 Coarse DNS at $Re_\tau = 180$

The first simulation presented is a coarse DNS of the channel flow at $Re_\tau = 180$ (the simulation number 1 in the table 4.1). This simulation is not strictly a DNS because, as it will be shown, for the numerical method in use, the grid is not sufficiently fine to obtain an error free simulation (as expected for a DNS); on the other hand, this is not even an LES because, as will be discussed below, the grid is fine enough that its associated projection error is practically negligible. Hence it can be assumed that this simulation is only affected by the numerical errors and as these errors will always be present in all the computations, it can be a useful reference for the following LES computations.

In this case, as in all the following LES simulations performed at $Re_\tau = 180$, the numerical solutions obtained with Fluent will be compared with the reference DNS solution of Moser, Kim and Mansour [29]. Their results were obtained with a full spectral code on a computational box of extension $4\pi H \times 2H \times 4\pi H/3$ discretized with $128 \times 129 \times 128$ grid points. The dimensions of the domain in the wall parallel directions were selected as the double of the distances over which the two point velocity correlations in the two directions become essentially zero (to ensure that the periodic boundary conditions are a proper choice); the number of grid points were determined by requiring that the smallest represented wavelength would have a negligible energy content. Hence to make a proper comparison, all the present simulations at $Re_\tau = 180$ have been made on a domain of the

same extension as in the reference DNS, as also reported in the table 4.1. Also for the coarse DNS presented in this paragraph, the grid adopted has the same resolution as the one in the reference DNS, in order to ensure that the simulation is not affected by the projection error of the grid.

The simulation has been performed with the second order central scheme, without any SGS model and the time step has been chosen to ensure that the time discretization error has a negligible effect with respect to the spatial discretization error (by making it much smaller than the viscous time scale). The initial condition for this specific case was obtained by zero-order interpolation of a previously performed LES computation of the same case (to be described later).

As the plane $y = H$ is expected to be a symmetry plane for the mean flow, all the quantities will be compared just for half channel height (in this as well as in all the other cases). In practice, this symmetry is never strictly achieved and the two half of the channel could have been used to perform an additional average of the quantities; however this has not been done as the number of samples selected for the ensemble averages was high enough that this additional average would have not yielded any significant improvement in the statistics.

Obviously, because of the limited space, it is not possible to present all the results for all the variables of interest in all the cases, hence only the most significant results will be presented, from which representative behaviors and effects are clearly recognized and which allow to discuss the effect of the numerical and physical parameters involved in the present investigation.

The first observation to note from these results is that not all the scales represented in the numerical solution are properly resolved. Two effects are clearly identifiable from the first plot. The first one is that, for the present numerical method, nearly two-third of the represented scales are affected by the numerical errors which act like an additional unknown scale separation operator and dump the highest represented part of the energy spectrum; however, as shown in the second plot, this error is not present in the span-wise spectra showing that this error, as expected, is connected to the directions of non-zero mean flow quantities (in addition to the fact that $\Delta z < \Delta x$). The second one is that even the scales which are presumed to be correctly resolved are actually affected by a slight under-prediction of the energy content. This could be recognized as an effect of the projection error, which therefore would not be negligible as expected. However, a grid independency study would be necessary to assess this, but it has not been done. The other two velocity components showed very similar behaviors hence they have not been presented.

The effect of the numerical errors can also be recognized in the mean velocity profile, represented in figure (4.4) together with the law of the wall $u^+(y^+)$. While the viscous sub-layer (up to $y^+ \cong 10$ is correctly resolved, mostly because the numerical errors act on scales which are already highly dumped by the viscous dissipation, this is not the case for the buffer and log layers. Indeed, the mean-velocity is under-predicted over the whole two ranges (which is represented by the under-estimation of the resolved part of the spectra) and the logarithmic behavior of the mean velocity is not recovered. Finally, the velocity

fluctuations profiles seem to be better represented, especially the wall-normal component, but the stream-wise and the span-wise components suffer, respectively, an under-prediction and an over-prediction in the middle of the buffer layer ($y^+ \cong 15 - 20$). While these results are of limited interest by themselves, they will be used in the following to infer about the role of the numerical method in the LES simulations.

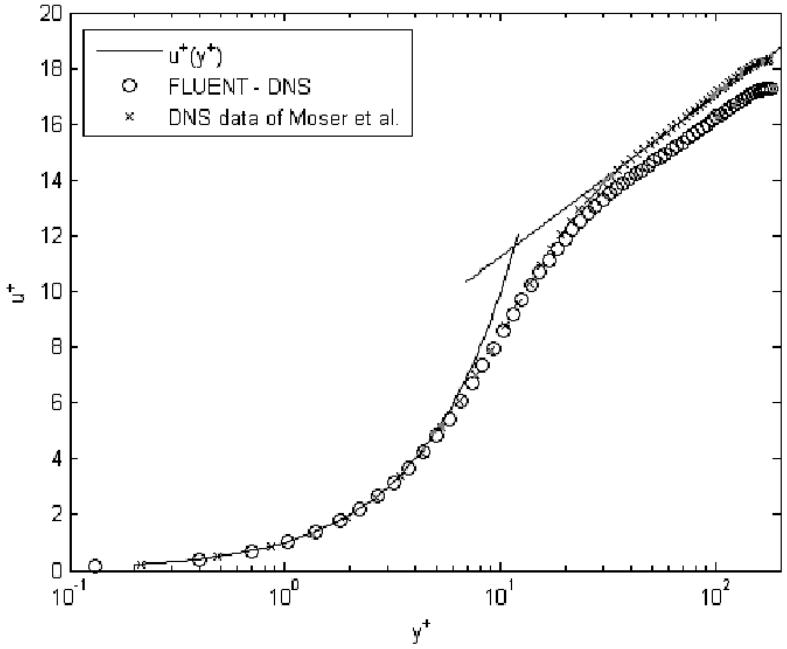

Figure 4.4: Comparison of the mean stream-wise velocity profiles in wall coordinates

4.2.3 Coarse LES in homogeneous directions

The first two LES computations analyzed are labeled 2 and 3 in the table 4.1. As it should be clear from the previous chapters, the LES in Fluent is simply realized by adopting a grid which is coarser than that required for a DNS but such that the energy containing range is at least represented (in theory it should be correctly resolved but, in practice, this cannot be guaranteed). Obviously, with respect to the DNS (which in Fluent is performed with the laminar viscous model, that is no model at all) a SGS model should also be selected to perform an LES computation. In this case, the grid is selected to have a resolution in the wall parallel directions which is much coarser than the one used for the coarse DNS, to properly establish the effect of the Fluent implicit filter due to the grid. In the wall-normal direction the resolution is instead similar to the previous case to avoid the additional error due to the non-commutation of the filter implied by the specific form of the dynamic model implemented in Fluent. The time step has been selected on the basis of the results of the previous chapter which showed that, for the numerical method in use, a Courant number $c \cong 0.1$ ensures that the time discretization error is overwhelmed by the spatial discretization one. Hence, for such Reynolds number, the dimensionless time step Δt^+ has shown to be strictly correlated to the maximum Courant number in the domain, the value $\Delta t^+ = 0.27$ has been selected as a good compromise; the effect of the time step on the LES results will be shown later. In both the simulations presented the initial condition was

obtained by a zero-order interpolation of a previously performed LES computation of the same case (to be described later) and the convective scheme selected is the second order central scheme to better compare these results to the DNS ones previously analyzed. The only difference between the two simulations analyzed here is in the SGS model used, which is the Dynamic Smagorinsky Model (DS) in the simulation 3 and no model at all in the simulation 2, like in the previous coarse DNS case.

According to these settings, it can be assumed that the no model computation is affected by the projection error, the numerical error and the modeling error while the computation with the model should try to reduce the modeling error. Obviously all these error components are supposed to interact, hence the scope of this comparison is to determine the effect of this interaction and the influence of the model in the reduction of the modeling error.

In the energy spectra, in addition to the considerations previously made on the numerical error (whose effect is still evident), two more aspects are worth highlighting. The first one is that, with respect to the coarse DNS case (which is also included in the figures for reference), here the grid has a clear cutoff effect as the range of represented scales is clearly smaller.

The second effect is that the smallest represented scales are clearly not dissipative enough (as well as the numerical method used) and the energy accumulates at the smallest represented scales. The interesting feature to note here is that this also happen when a supposedly appropriate SGS model is used, which should dissipate the correct amount of energy, and actually there is no appreciable effect of the model on the energy spectra (these effects are also recognizable in all the other spectra not presented here). This could depend on two factors. The first is clearly the fact that the SGS model is of the same order as the truncation error, which therefore has a bigger effect. The second is that the DS model is mostly sensitive to the smallest represented scales, which also are the most affected by the numerical error, hence the model could be further disadvantaged by this.

In contrast, the model has a still appreciable (but limited) effect on the mean velocity profile. However, as it clearly appears, the major effect on the mean velocity profile is determined by the total scale separation operator acting on the solution, determined by the grid and the numerical errors. Indeed, while the logarithmic behavior is still missing (which suggests that the actual wall-normal resolution could just be not sufficient to represent it as this error seems to be independent from the wall parallel resolution and the modeling approach), now both the LES computations largely over-predict the mean velocity profile over the buffer and log layers. However, it can be argued that this is mostly due to the large projection error as this is an effect also present in several explicitly filtered LES computations (in which the numerical errors are made negligible; among the others, see [55][49]). The same is also valid for the large over-prediction of the r.m.s stream-wise velocity fluctuations. Hence, the effects of the projection error on these statistics, for such a coarse grid, clearly overwhelm those due to the numerical error (which is instead dominant on the spectra). The SGS model effect can still be recognized in the figures (4.5) but again it is only a limited effect and it is suspected that most the error in these fluctuations too is still related to the projection one.

Finally, the behavior of the mean turbulent viscosity ratio for the simulation 3 is presented (from which it is clear that the model dissipation is irrelevant with respect to the viscous resolved one) and it is shown that the expected near-wall y^3scaling of the dynamic SGS viscosity is correctly recovered (up to the inevitable numerical errors which overwhelm it in the close proximity of the wall). As this behavior is recovered for all the computations, it will not be presented anymore.

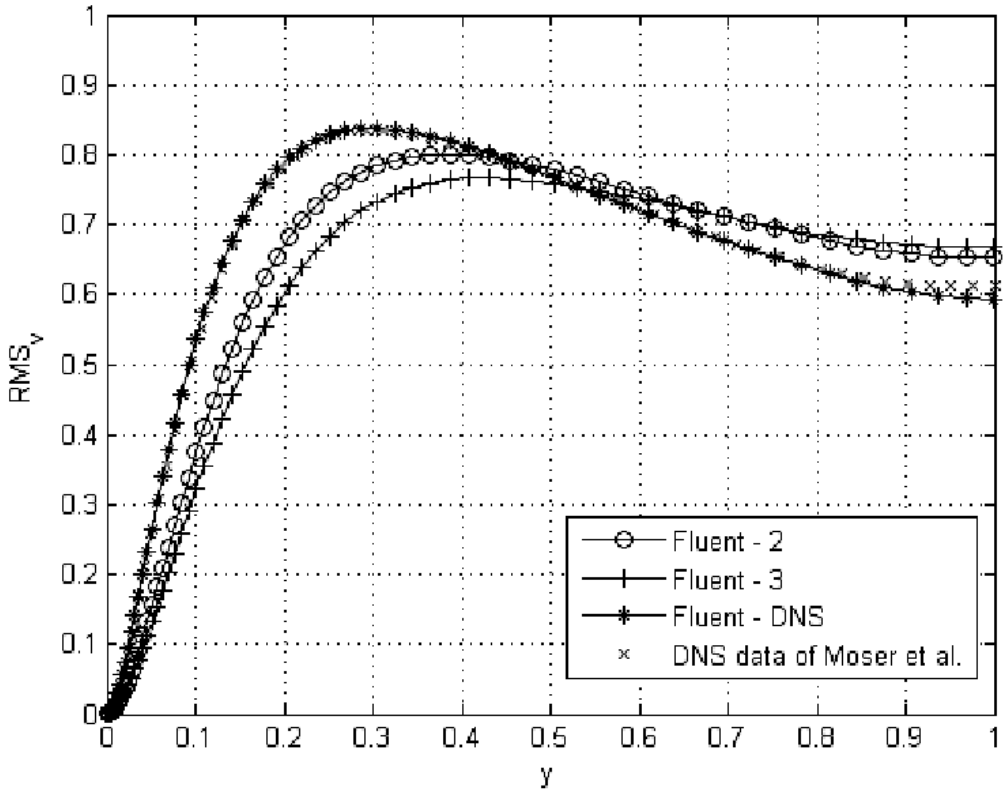

Figure 4.5: Comparison of the r.m.s wall-normal velocity fluctuations

4.2.4 Effect of the resolution and the SGS model.

To better investigate the effect of the grid and the SGS model on the numerical results, the next comparisons will be made at an even different resolution for different SGS models; in particular, the simulations 7, 8 and 9 will be analyzed.

As these were the first simulations made, it was necessary to specify a proper initial condition. According to the explanation given in the chapter 2, as the interest here is in the statistically steady state only, the main aim of the initial condition is to reach it as quickly as possible. Among several possible choices, the initial condition has been chosen to be a randomly perturbed laminar velocity profile. This is not the best possible choice (as there is no control on the initial transient time) but as it had to be used only once (the other simulations being initialized with previously computed velocity fields), it was considered appropriate.

The grid has been chosen to be representative of a wall-resolved LES hence, with respect to the previous analysis, the resolution in the wall normal direction has been halved while the wall-parallel resolution has been increased. Also, the time step has been kept fixed with respect to the previous case. These simulations are certainly more complex than the previous ones because, in theory, all the errors are now relevant, including the commutation error connected to the dynamic models (as the resolution in the wall-normal direction is now connected to a projection error).

The first aspect to note is that all the three simulations (which only differ for the SGS model employed) give nearly the same results for the spectra as well as for the other quantities (only a limited set of results is presented here as all of them yields the same conclusions), the only difference being in the values of the SGS viscosity and the slight under-estimation of the velocity profile for the no-model simulation. Also the logarithmic behavior is still not fully recovered by any of the simulations.

Several effects are recognizable in these behaviors. First, it is clear that the SGS model is almost completely overwhelmed by the numerical error, whose predominant effect is evident in the spectral energy distribution. The effect of the SGS model is slightly evident in the mean velocity profile, but only with respect to the no-model simulation as there is no clear difference between the two SGS models compared (DS and TKE). However, by comparison with the results of the previous analysis, it is clear that the dominant role in the prediction of the velocity profile is played by the projection error, as now it is correctly predicted. Therefore, it can be concluded that the role of the SGS model is very limited and independent from the specific model, probably because it is dependent on a spectral band which is dominated by the numerical error. Also, it is evident that the numerical error prevents the role of the SGS model from becoming relevant with increasing projection error, as the effect of the model seems to be the same independently from the resolution.

The only relevant difference between the two SGS models is in the value (but not the behavior) of the SGS viscosity which nonetheless are both irrelevant with respect to the viscous one. The lower value for the TKE model is explainable by the fact that its SGS viscosity is determined by the SGS kinetic energy and not by the dissipation at the test filter level.

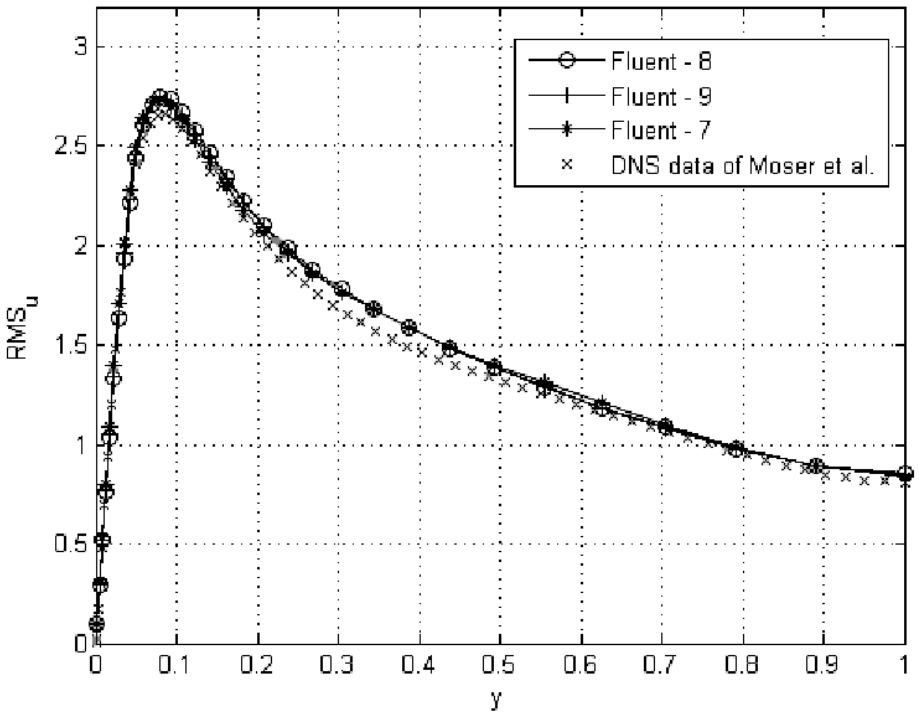

Figure 4.6: Comparison of the r.m.s stream-wise velocity fluctuations

4.2.5 Effect of the Convective scheme

In the previous paragraphs, it was shown that the LES computations in Fluent are mostly affected by the numerical method, hence it is fundamental to determine how the results are affected by the other convective scheme supposed to be suitable for LES computations, the bounded central (BC) scheme. Therefore, in this comparative analysis, the simulations 10 and 11 will be compared to the simulation 8, assumed as the reference one. The grid and the time step are as in the previous case and the initial condition of the simulation 8 has been used for all the cases.

The BC scheme belongs to a class of schemes originally developed for the numerical solution of the compressible Euler equations and for interface-tracking applications; these schemes are designed to introduce a certain amount of dissipation that adapt itself to the energy flux toward the smallest represented scales and forces the solution to remain bounded (to cure the non-monotone behavior of high order schemes and preserve some physical constraints of the shocks). In practice, the modified equation analysis shows that the leading term of the truncation error of these schemes closely resembles a general tensorial sub-grid viscosity model [33][48][18]. Thus, the use of such a scheme can be considered as an implicit functional modeling approach.

When the results for this scheme are analyzed, its features can be clearly recognized. Indeed, from the stream-wise spectra it is evident that the solution is sensitive to this added dissipation while it is not sensitive to the dissipation of the SGS model (whatever the convective scheme used is). However, as for all the other cases, this effect is not present in the span-wise spectra.

In addition to this, the BC scheme also has a more subtle effect. Indeed, the added dissipation of the scheme acts like an additional implicit scale separation operator (with respect to the one determined by the grid and the central scheme) which, while being still connected to grid, has a dominant effect. This can be partly deducted from the stream-wise spectra but it is mostly evident where the typical over-predictions in the velocity profile and in the stream-wise velocity fluctuations can be recognized. As explained before, this effect seems to be due to a large scale separation error which, by comparison with the simulation 8, can clearly be connected to the dissipation of the BC scheme.

Finally, in figure (4.7), the SGS viscosity ratio profiles for the two schemes are compared. In both cases, the solution is not sensitive to the SGS model but the additional dissipation of the BC scheme is felt by the dynamic model, which yields lower values for the SGS viscosity.

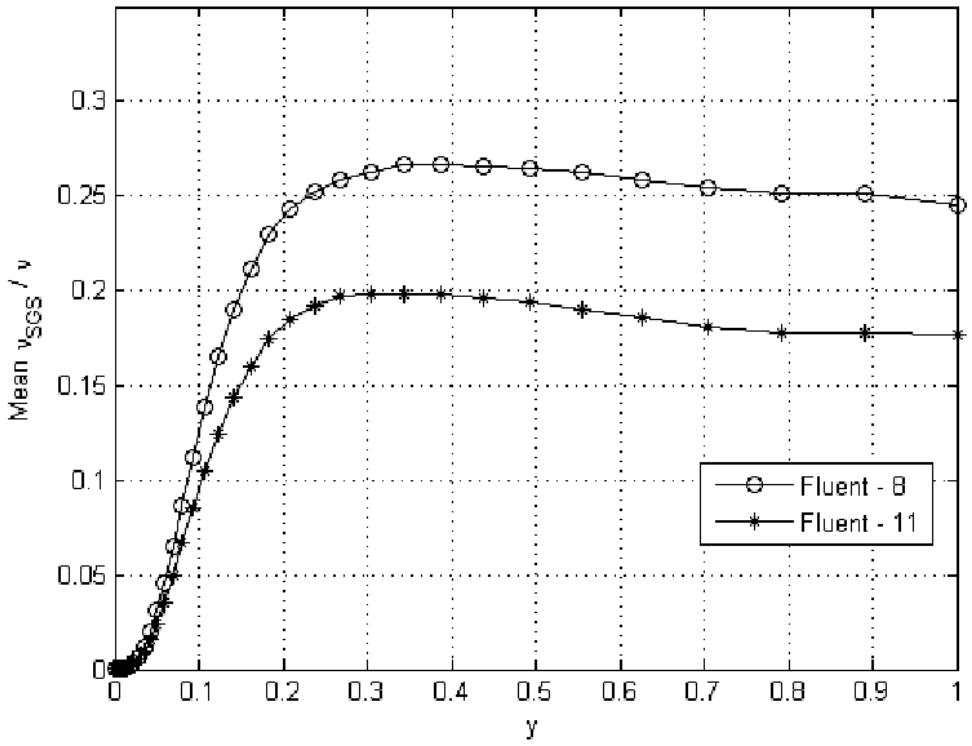

Figure 4.7: Comparison of the mean SGS viscosity ratio profiles

4.2.6 Effect of the Time Step

The last numerical parameter whose effect needs to be investigated is the time step. In all the previous computations, it has been kept extremely low, to avoid the effect of the time discretization error, but the adoption of the second order implicit scheme allows in principle the selection of much higher time steps. Therefore, the aim of this confrontation is to establish in which range of values the time step can be chosen without incurring the additional time discretization error and if any what is its effect on the numerical solution. However, it is worth remembering that it has been shown that the courant number, while not being limited by the stability issues, is instead subjected to an accuracy related restriction. For the present analysis, the solution 5 and 6, with $\Delta t^+ = 0.9$ (and the

associated Courant number $c \cong 1$), have been compared to the reference solution 11, with $\Delta t^+ = 0.27$. This is the only comparison made, as it clearly suggests that even such a small time step has a big influence on the LES results. There are two main reasons for this. The first one is in the results of the simulation 5, mostly the spectral energy distribution. Indeed, it shows that the effect of the increased time step is to induce an energy accumulation at some of the represented frequencies, but not the highest ones.

This somehow suggests that the implicit filter induced by the time discretization error has a cutoff length which is larger than the one connected to the grid. The span-wise spectra instead, as in all the previously analyzed cases, are not affected by this behavior. However, this additional induced filter seems to have an effect even on the mean velocity profile and the velocity fluctuations, as the simulation 5 has a behavior which is very close to the simulation 11.

The second reason is that the energy accumulation can be effectively avoided with the BC scheme (simulation 6) but this introduces an additional scale separation effect with respect to the simulations 5 (in the velocity profile and in the velocity fluctuations) and 11 (in the stream-wise spectra).

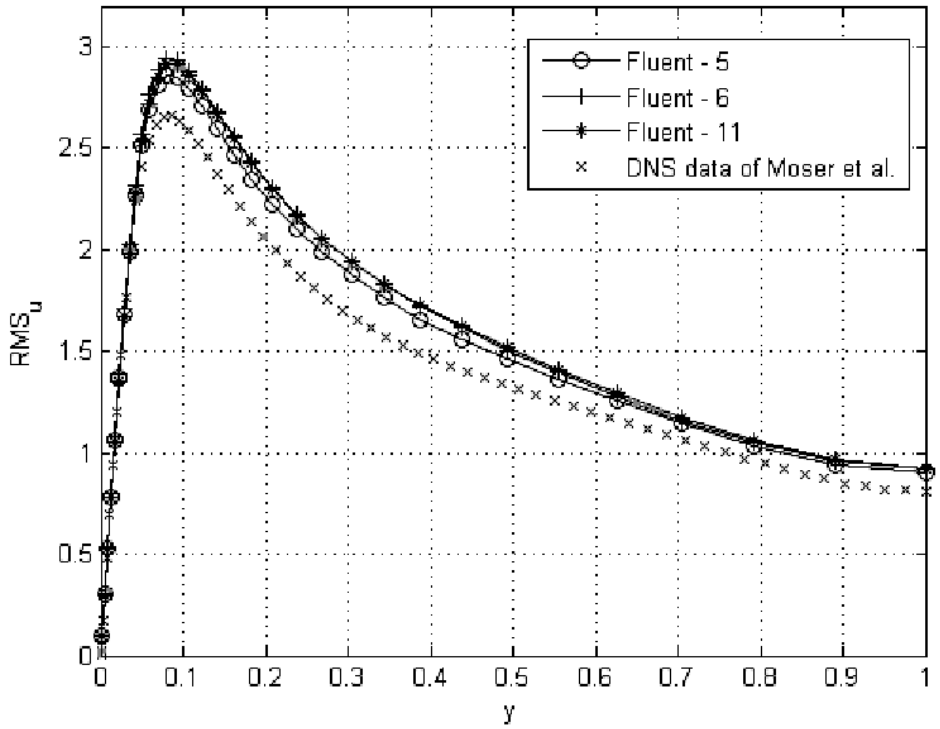

Figure 4.8: Comparison of the r.m.s stream-wise velocity fluctuations

4.2.7 Coarse LES at $Re_\tau = 2000$

The cases previously considered, while being very common in LES validations and useful to assess the numerical dependencies of the LES results, are not even close to be representative of a real LES application. The main reasons for this are the low Reynolds number of the simulations and the simple geometry of the case. As a consequence, a

simulation with a higher Reynolds number has been considered. The solver has been tested with its basic wall-modeling approach, which is based on the classical wall-functions [28]. The solver also has other near-wall modeling approaches but it is believed that the basic one is more representative of practical cases as it is automatically turned on wherever necessary in the domain.

The numerical solutions obtained with Fluent are compared with the reference DNS solution of Hoyas and Jimenez [56], obtained with a de-aliased pseudo-spectral code on a computational box of extension $8\pi H \times 2H \times 3\pi H$ discretized with $6144 \times 633 \times 4608$ grid points. In contrast to the previous cases, it has not been possible to use for the test a domain with the same extension of the reference DNS one as it would have required a huge amount of computational resources, even with the wall-modeling approach. As a consequence, the present simulations (number 12 and 13 from table 4.1) have been performed on a domain of extension $2\pi H \times 2H \times \pi H$, which is comparable to the extension used by other authors in LES computations of the same case [40].

An uniform grid with $64 \times 65 \times 64$ points has been used for the domain discretization while the time step has been fixed to $\Delta t^+ = 0.3$. In viscous units, it is comparable to the previous cases but, for such a grid and Reynolds number, it leads to a much smaller Courant number.

Two kinds of effects can be recognized from the present results. The first one is connected to the low resolution of the grid (i.e., the high number of missing scales) and the even lower one determined by the use of the BC scheme, which clearly appear from the energy spectra. Also, the logarithmic behavior is till not correctly recovered (even if the wall-modeling approach enforces a correct value of the velocity in the first cell of the wall). Moreover, in very contrast to the use of the BC scheme, it is evident that the SGS model is still ineffective in providing the correct amount of dissipation when the central scheme is used, as dramatically shown by the energy accumulations in the spectra for the case 12. Even if not presented here, it is interesting to mention that the higher projection error of this case also leads to higher values of the mean SGS viscosity ratio, with a maximum of nearly 4 (that is approximately 10 times higher than in the previous low Reynolds number cases).

It can be seen that the selected wall-modeling approach, while being effective in the description of the velocity profile, does not properly represents the velocity fluctuations. As discussed before, this is not the effect of the specific wall-modeling approach used in Fluent but it is a common feature of all the wall-stress modeling approaches. In practice, as these models are not usually different from those used in the RANS approach, they are not specifically designed to determine the amount of resolved scales at walls (and the fluctuations connected to them). Hence it seems that all the fluctuations are resolved on the coarser grid without consideration of the modeled part.

4.2.8 Conclusion from the channel flow test case

The most influencing factor is the total scale separation determined by the numerical error and the projection error of the grid. Indeed, while there is a clear effect due to the changes in the resolution (projection error), all the results are influenced by the numerical error.

This is valid not just for the BC scheme but even for the pure central scheme, both making the solution insensitive to the specific SGS model used. It is not clear how much this is influenced by the error introduced in the application of the dynamic procedure but it is evident that the spectral resolution of the two schemes is only slightly different; moreover this difference is fully concentrated in a part of the spectra which is not correctly resolved by both of the schemes.

In practice, the previous analysis suggests that, independently from the convective scheme used, only $1/5$ of the represented scales are correctly resolved and the presence of a SGS model only slightly influences the mean velocity profile but it is not effective in its main role of providing the correct amount of dissipation. As a result, it seems reasonable to adopt the ILES approach, that is the BC scheme without any SGS model. It follows that the minimum grid requirement for a correct LES application in Fluent can be estimated to be:

$$h = \frac{\ell_{EI}}{10} = \frac{L}{r \cdot 10}$$

where h is the minimum grid step required, L is a geometry dependent length (relative to the flow region to be discretized) and r is a flow/region dependent parameter.

The use of the BC scheme prevents the energy accumulation at intermediate scales due to the implicit filter induced by a too much high time step. It follows that, when the BC scheme is used, the main limitation on the time step comes from the accuracy requirement.

Finally, the use of the wall functions in Fluent seems to be affected by the same features of the most common wall-modeling approaches in LES and their use should be avoided unless the computational requirements become unaffordable.

Chapter 5

Simulations on a confined, swirled jet

5.1 Introduction

The main objective of this chapter is to implement the LES approach to a swirl combustor for two different swirl numbers and keep modifying the geometry so as to obtain an accurate solution which is very close to the LDV and PIV experimental results. The approach is to provide inlet mass flow rates where usually known, include the full swirl generation device in the computation and let the swirl number be determined by the computation. The main advantage of this approach is that is is not dependent on any external information besides mass flow rates.

After validating the LES model in a test case, two simulations with different axial and tangential mass flow rates (overall sum being the same) were performed. The two different mass flow rates were 390(Tg)-50(Ax) and 200(Tg)-240(Ax).The flow is governed by S at the annular exhaust into the chamber.

$$S = \frac{\int_0^R UWr^2\, dr}{R\int_0^R U^2\, r\, dr}$$

In general, several flow instabilities such as vortex breakdown are present. It is a well known fact that the exit boundary conditions have a tremendous influence on the recirculation zone. Hence the geometry needs to be modified, especially on the exit section, so as to find an accurate numerical solution. The flow parameter ($Re_{D_e} = 22600$) is the same in all the domains. The statistical data was accumulated. The mean flow results were investigated in terms of velocity field, turbulence quantities and volume flow rate. The presence of the unsteady flow features was also investigated. The initial geometry of the swirl combustor, which has 4 tangential inlets and 4 axial inlets, modeled using Gambit is as follows:

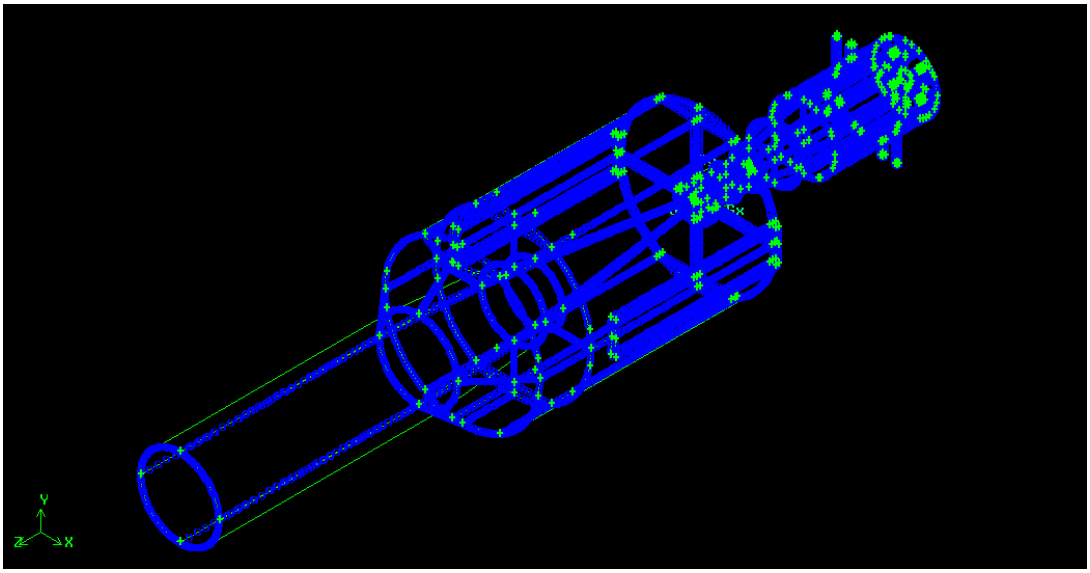

Figure 5.1: Initial Geometry of the Swirl Combustor (Isometric View)

5.2 Computational setup

5.2.1 Mesh description

The YZ cross section of the full size mesh of the final geometry can be seen in fig.: 5.2. Hex-map approach was used for most parts of the geometry except the central cylindrical part. Since it is connected to specific flow features in different parts of the flow, specific mesh sizes were given for different parts of the domain. It is important to prevent mesh distortions in order to use a proper pressure and convection schemes.

5.2.2 Boundary Conditions

The shear in the lateral wall of axial and tangential inlets was specified zero. The mass flow rate boundary condition was given to the inlet, normal to boundary. The gas gun inlet was switched to wall to avoid possible problems. Pressure outlet with average pressure specifications was given at the outlet section. Finally two planes were created to check the initial condition in the domain which is also useful for the post processing needs.

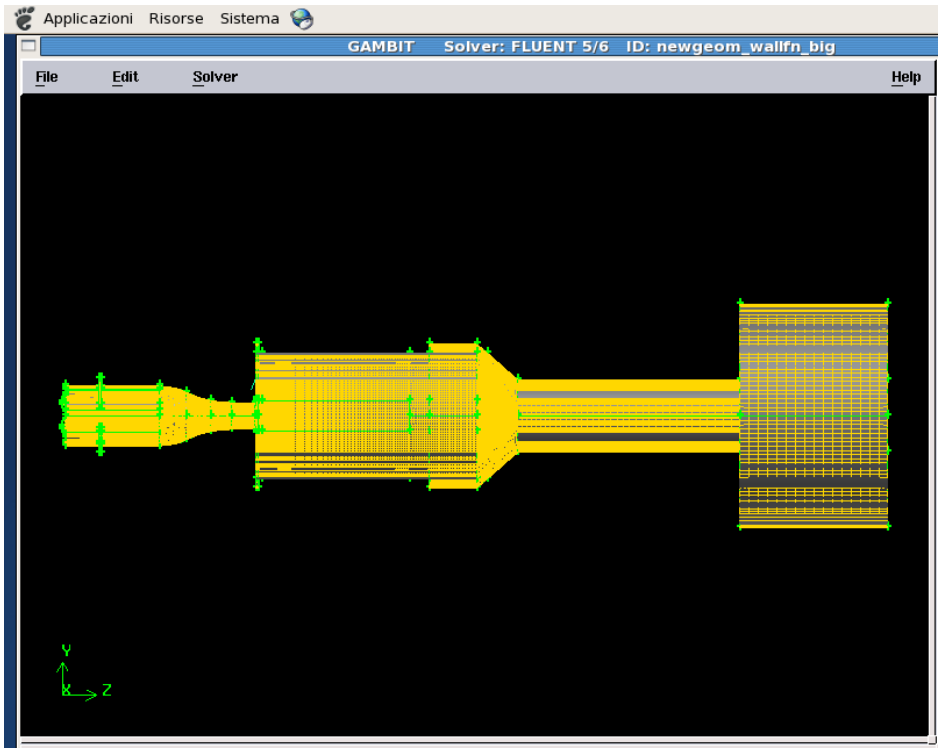

Figure 5.2: Final Meshed Geometry in the YZ plane

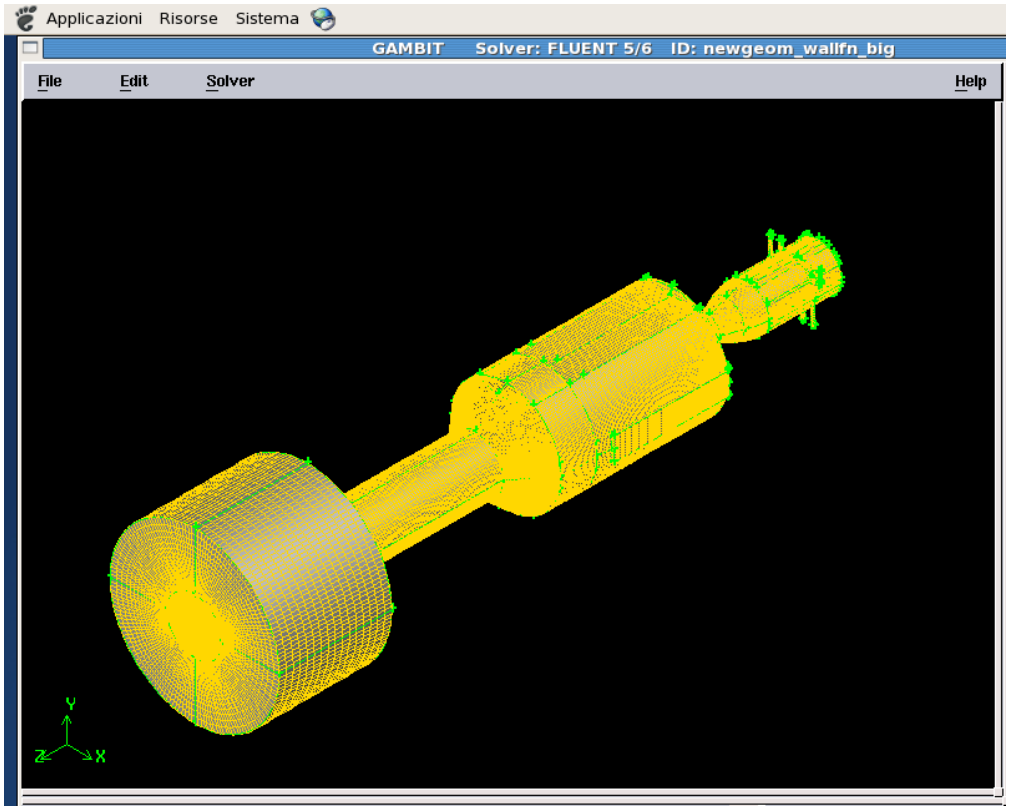

Figure 5.3: Isometric view of the final meshed geometry

5.2.3 Numerical Parameters

Once the mesh is read in Fluent, the model setup is done. The flow is unsteady and the viscous model chosen is LES with Dynamic Smagorinsky model. Both the simulations for all the domains are performed by Non Iterative second order implicit time advancement, with Bounded Central Difference Scheme for the convective term, and Linear scheme for the pressure. Initially Presto was used but was found to be unstable for non-orthogonal grids. For the pressure velocity coupling, Fractional Step method was used. Time step was chosen to keep the CFL number below 0.8 . Computations were started from the zero initial conditions for all variables ($u = 0, v = 0, w = 0, p = 0$). A field function was defined based on energy norm to monitor in time the evolution of the flow. Averaging started when turbulent flow was developed, and statistical data was accumulated.

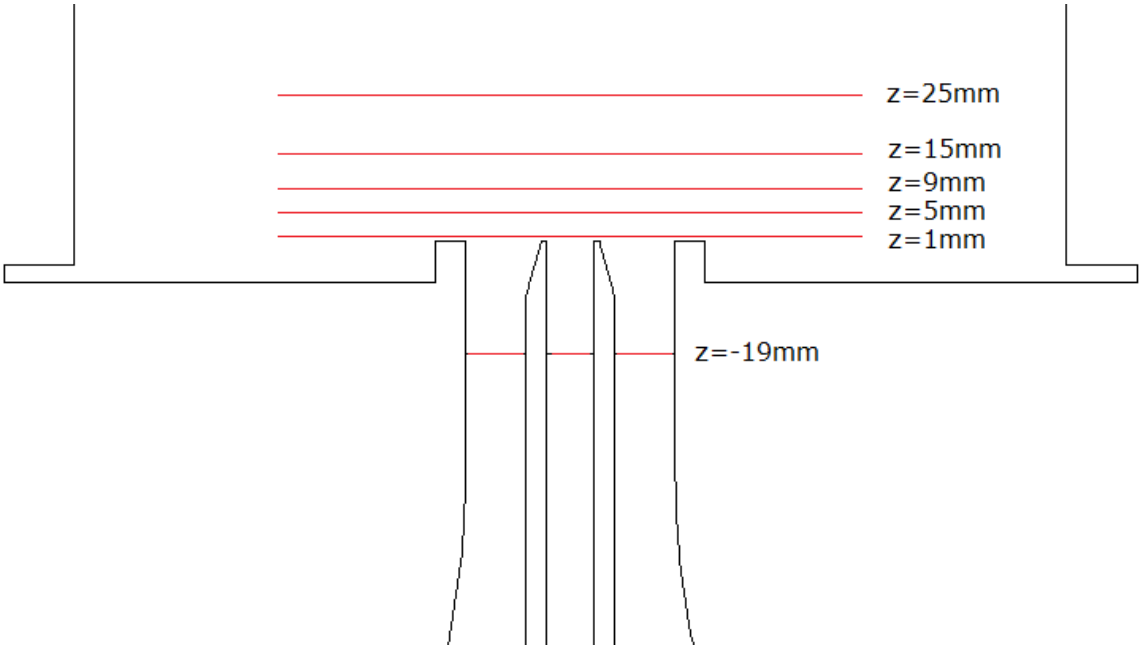

Figure 5.4: Different Lines at outlet sections for comparison of results

5.3 RMS Velocity Magnitude results

In this section, the results for both the cases for final geometry configuration are plotted. The maximum r.m.s velocity obtained for the first case is 17.4 m/s near the inlet region whereas it is 13.9 m/s for the second case with tangential mass flow rate = 200 Nl/min and axial mass flow rate = 240 Nl/min.

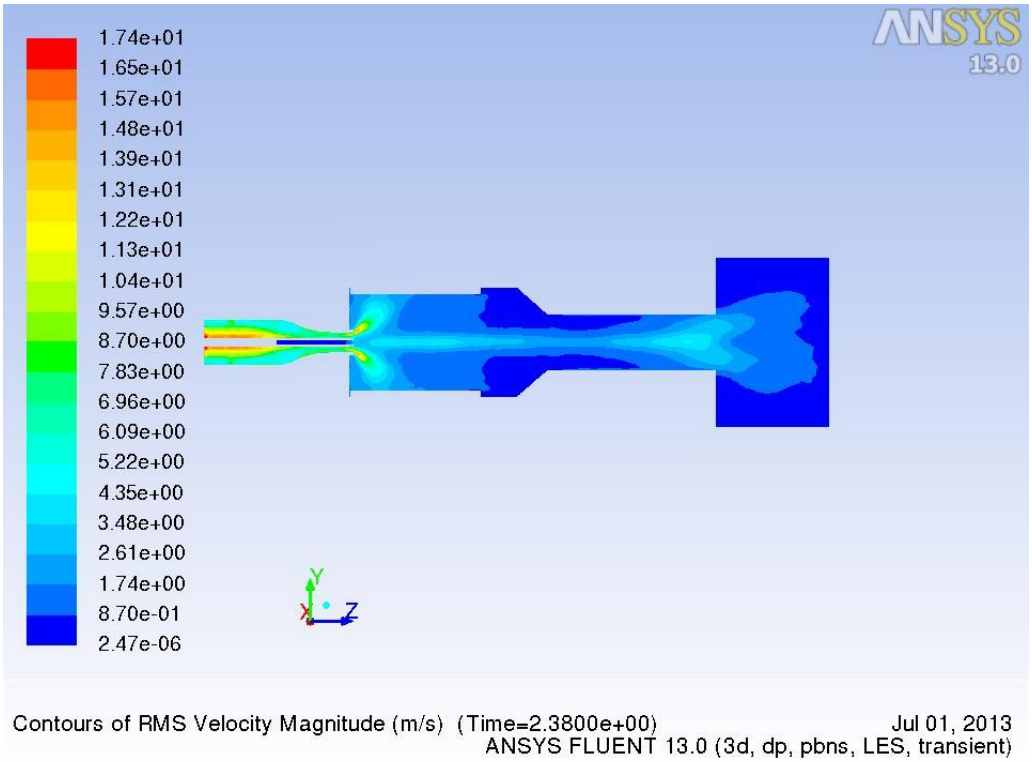

Figure 5.5: Contours of RMS Velocity Magnitude (390-50 case)

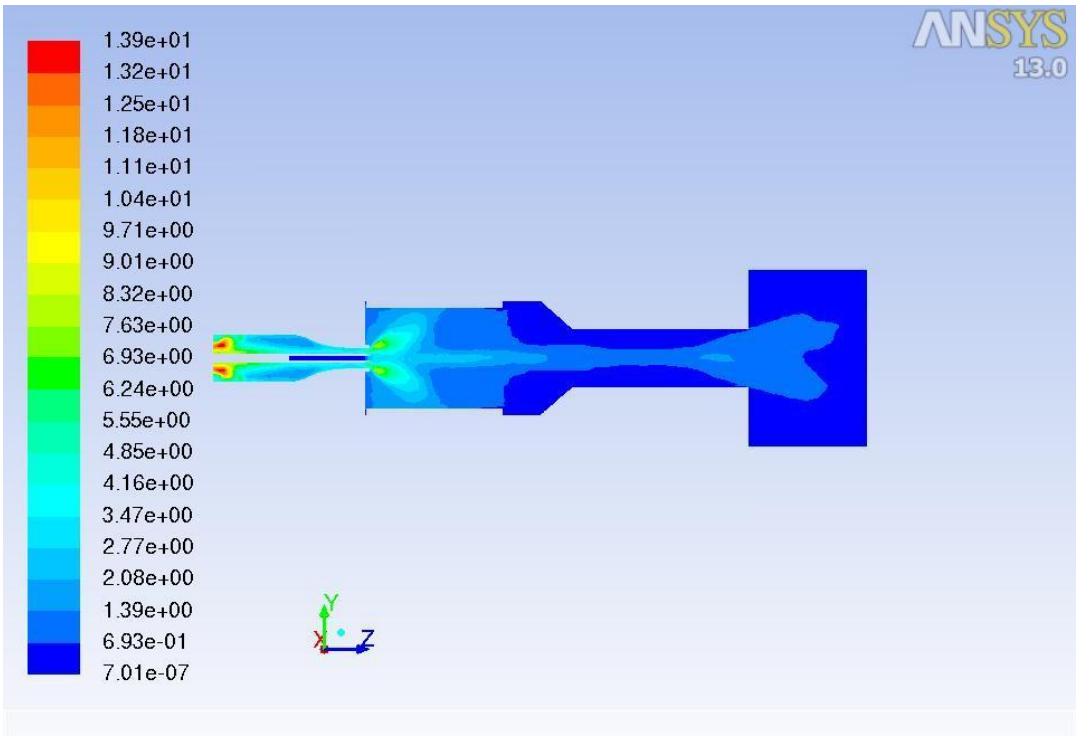

Figure 5.6: Contours of RMS Velocity Magnitude (200-240 case)

Comparisons between experimental and numerical solution for

Case 1 (390Tg - 50Ax)

<u>At Z = +5 mm</u>

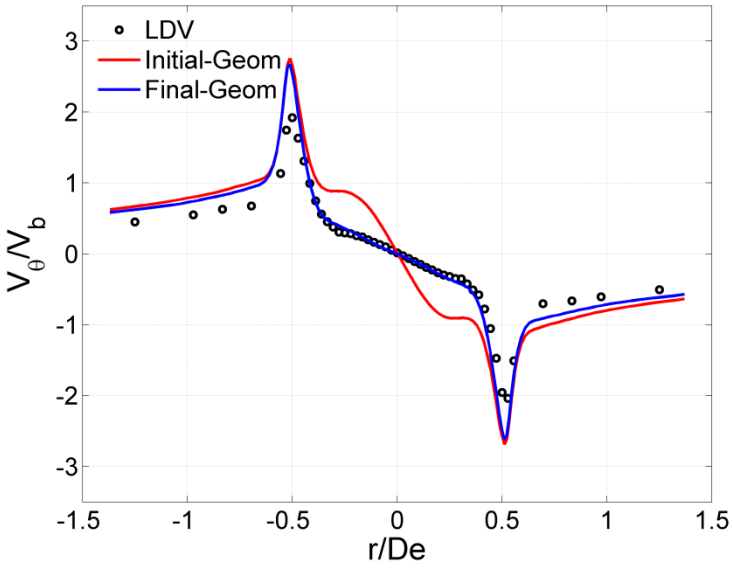

Figure 5.7: Radial profile of the time-averaged tangential velocity component at Z = +5 mm

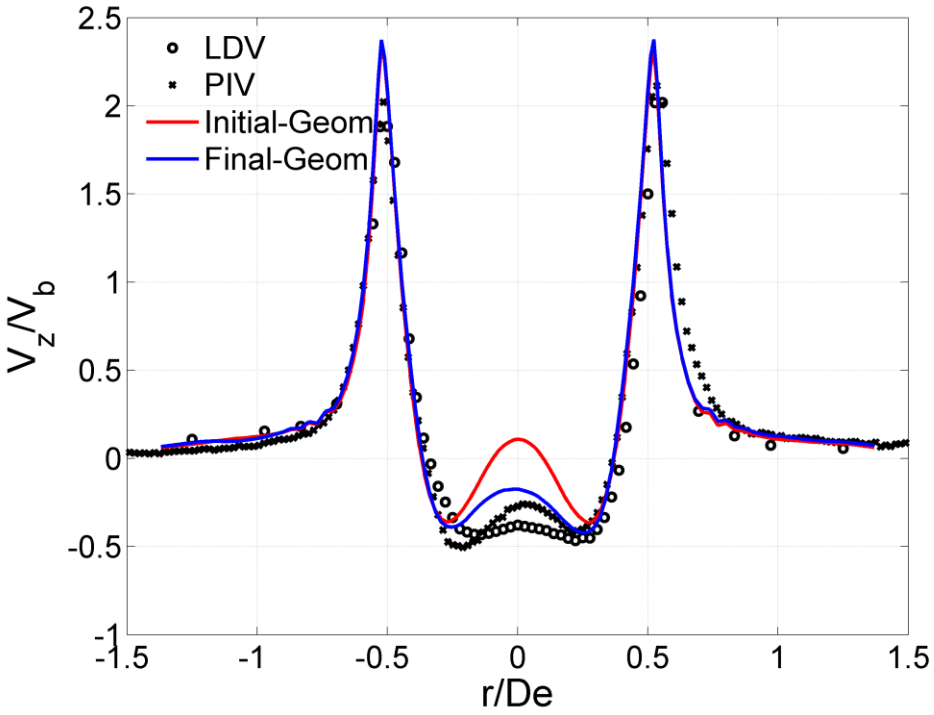

Figure 5.8: Radial profile of the time-averaged axial velocity component at Z = +5 mm

The comparisons with the experimental data are shown in Figures 5.7 and 5.8. Here V_b is the bulk velocity. The time-averaged mean axial and tangential velocity profiles are plotted. The time-averaging calculation was performed using about 100k time steps, which was shown to give a converged time-average. The overall agreement between the experimental and computational results is good.

An axial force is used to represent the mean pressure gradient that drives the main flow and an azimuthal body force is used to overcome the drag from the walls and drives the azimuthal flow.

As shown in Figures, due to the centrifugal force generated by the swirling motion, the center fluid forced to move outward, and it results in a decrease of the axial velocity in the inner part near the axis and an increase in the outer part. Additionally, the sudden expansion at the end introduces another axial velocity deceleration. The radial pressure gradient is proportional to the outward centrifugal force.

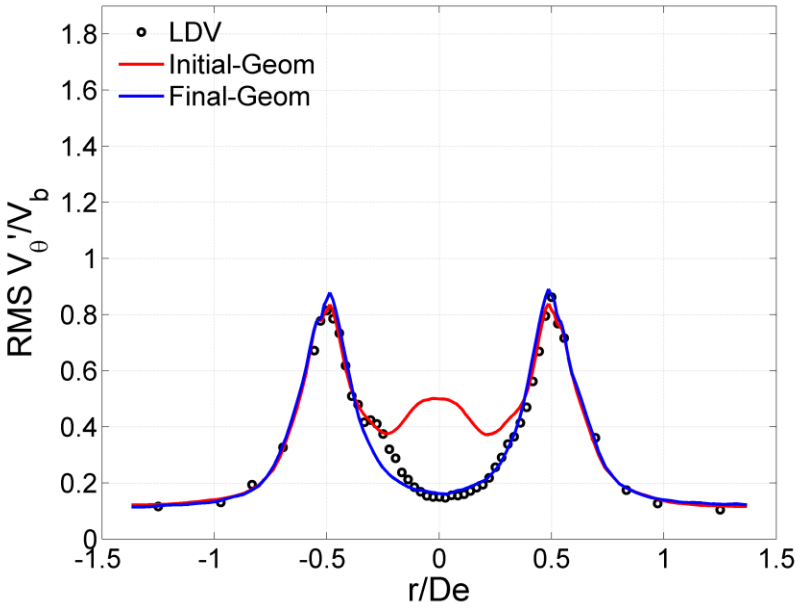

Figure 5.9: Radial distribution of the normalized intensities rms of tangential velocity fluctuations

Along the axial direction downstream, the axial and the tangential velocity profiles become smoother. Both the axial and the tangential velocity components are significantly lower than the peak values upstream at the farther end. This is due to the high spreading rate of momentum in swirling flows. High spreading rate is an important property of swirling flows. In combustion systems, it is often used to enhance the mixing of the reactants.

At Z = +9 mm

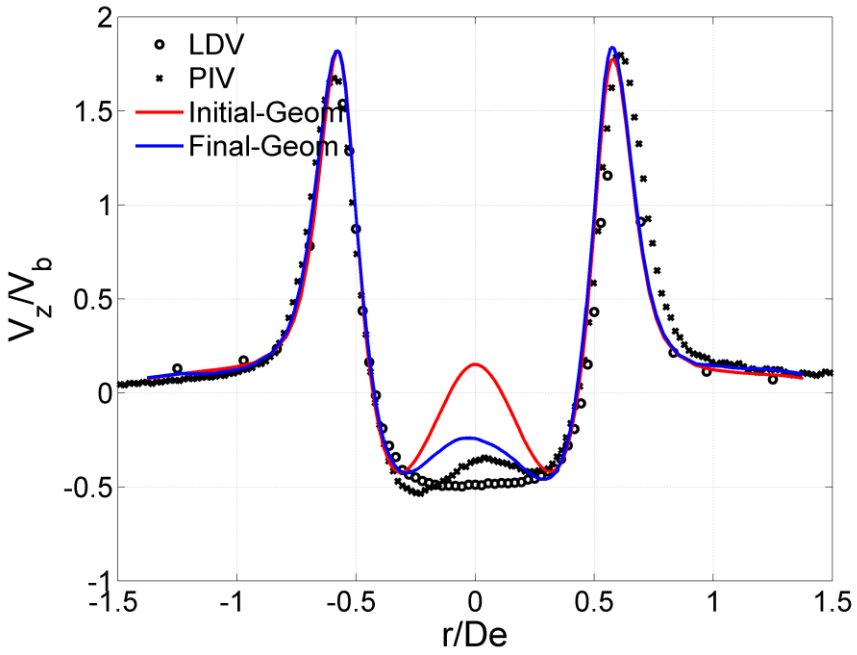

Figure 5.10: Radial profile of the time-averaged axial velocity component at Z = +9 mm

At Z = +15 mm

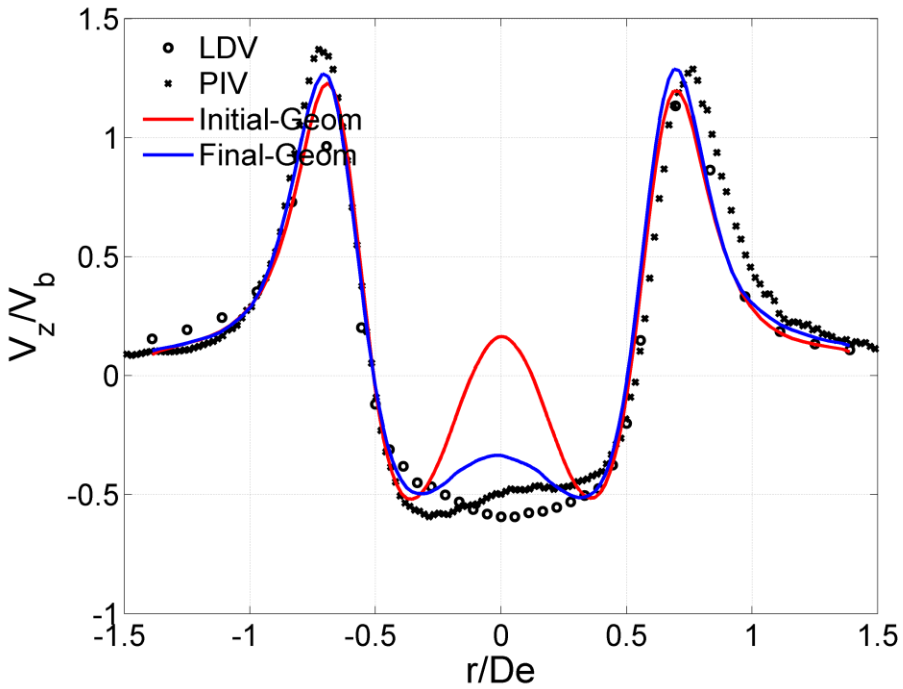

Figure 5.11: Radial profile of the time-averaged axial velocity component at Z = +15 mm

The above graphs are radial distribution plots. The experimental LDV and PIV data are compared against the numerical solutions. Since the geometry was modified to obtain a closer solution, both the results have been plotted. From the plots, it can be clearly seen that the numerical LES computations are very accurately matching the experimental results.

Comparisons between experimental and numerical solution for

Case 2 (200Tg - 240Ax)

At Z = +5 mm

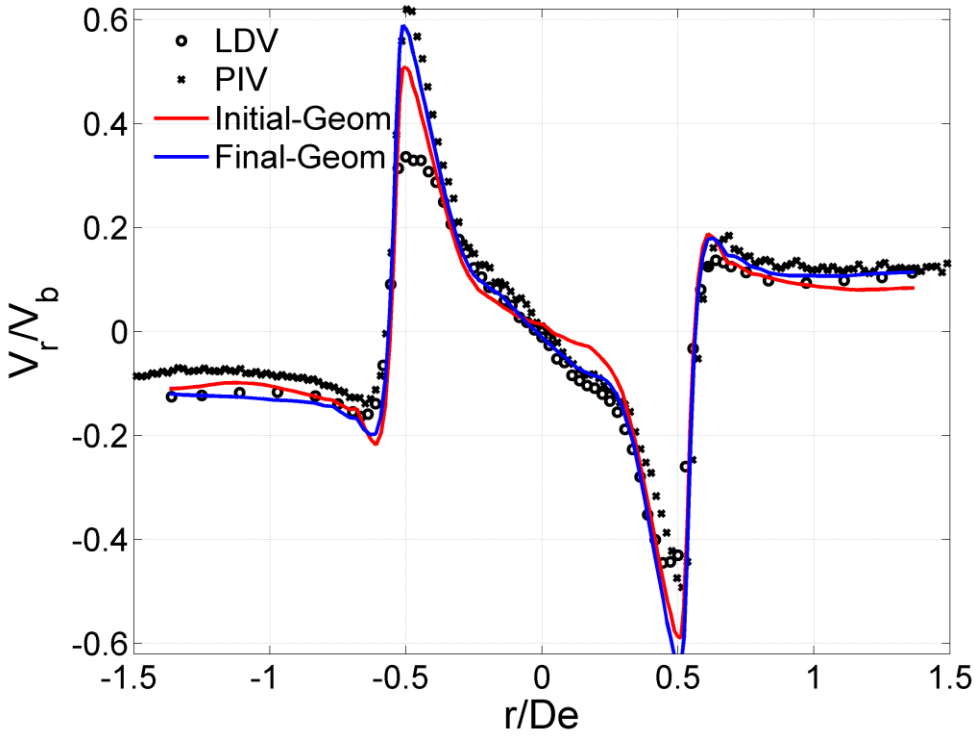

Figure 5.12: Radial profile of the time-averaged radial velocity component at Z = +5 mm

At Z = +1 mm

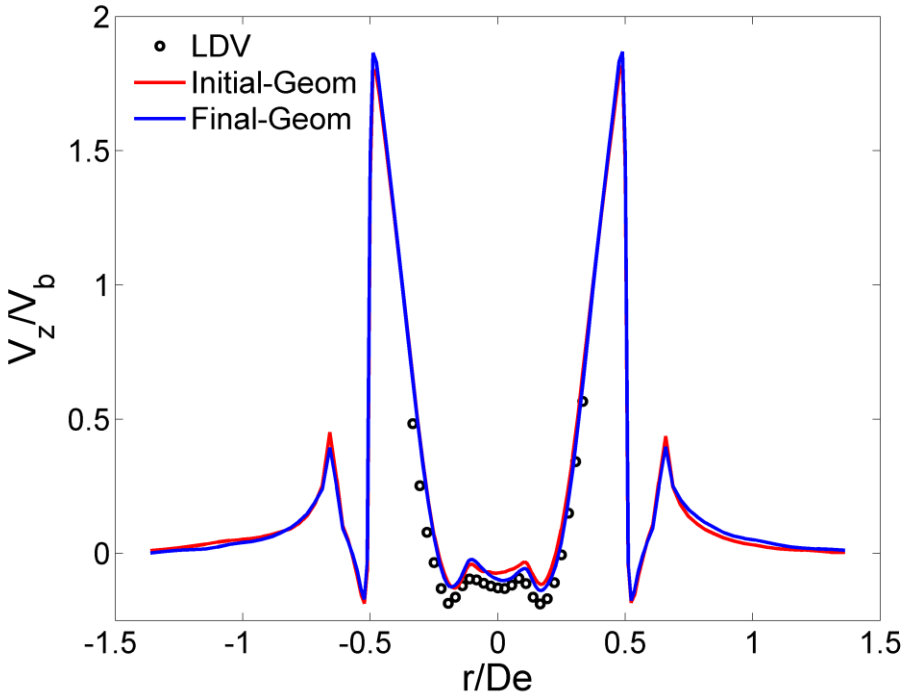

Figure 5.13: Radial profile of the time-averaged radial velocity component at Z = +5 mm

The above results suggest that the influence of outflow boundary condition depends strongly on the swirling flow structure itself. For lower swirl number flows without the vortex breakdown, the influence of the outflow condition is very limited. With stronger vortex breakdown, the influence of the outflow boundary condition can be fairly strong and it affects almost all the flow field.

The main difference between initial geometry and final geometry is the outlet part. One may expect that the outlet geometry has an effect on the flow structure as the outflow condition does. Basically, it can be considered as two different outlet configurations. The effect of the outlet configurations can be clearly seen in the above plots since it has resulted in a more accurate solution as the experimental results. At far downstream, the effect of the outlet geometry is more noticeable. The agreement of the calculated mean axial and tangential velocity with the experimental data is good.

The differences are not as much correlated on the velocity profile at inlet as on the flow development in the chamber. The axial plot of the swirl number can show the changes in the Z direction more clearly. The comparisons show that the overall flow structure is different as the central recirculation zone assumes a different size and axial length. This has an impact in combustion applications.

5.3.1 Results in the centerline

The decaying properties of the jet are in good agreement with the measurement data. In terms of the u_{rms} in the centerline, there is also no clear difference between the two simulations. The maximum rms value of 0.45 was found at $r/De = 0.4$ However in the decaying turbulence region the averaging time for statistics seems to be insufficient because the u_{rms} graphs are not smooth (do not forget that the spatial averaging in the azimuthal direction does not improve the turbulence statistics in the centerline, where the radial coordinate is zero $r = 0$). In the decaying region, the agreement of the measurement and simulation data is satisfactory, concerning that the statistics are not fully converged.

The good agreement between the simulations with different streamwise length of the meshes, provides an opportunity to test the boundary conditions (especially the inflow boundary) and the numerical parameters on the short mesh efficiently, with less computational effort. After this testing the good configurations can be transmitted to the long geometry, as it was done in this study.

5.3.2 Instantaneous flow features

The instantaneous flow features are described in this section, which provides a picture of the time dependent flow topology. The flow structures were detected with the help of Q, λ_2 and p' criteria.

Q criteria

The value of Q [64] is the second invariant of the velocity gradient tensor. It can be calculated as:

$$Q = \frac{1}{2}\left(\Omega_{ij}\,\Omega_{ji} - S_{ij}\,S_{ji}\right)$$

where, $S_{ij} = \frac{1}{2}\left(\partial_i u_j + \partial_j u_i\right)$ is the rate of the strain tensor and $\Omega_{ij} = \frac{1}{2}\left(\partial_i u_j - \partial_j u_i\right)$ is the vorticity tensor. In figure 5.21 we can see the Q isosurface. Both small and large structures can be seen. The small coherent structures are dominant at the inflow, and downstream in the decaying region the larger features became visible at the side of the shear layer.

In the centre plane of the jet we can see that the Q structures begin to develop very close to the exit plane of the jet. Because the rolling up of the shear layer began near to the exit it is obvious that the gas gun geometry could affect the creation mechanism of the coherent structures.

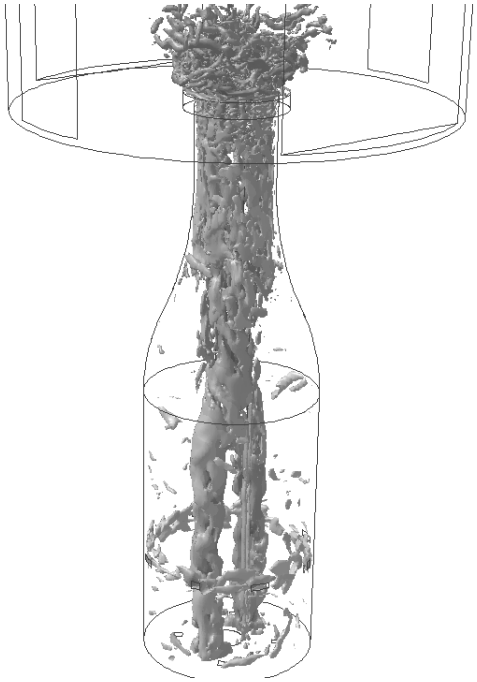

Figure 5.13: Q isosurface with streamwise vorticity

Time scales

Considering the motion of the structures in a sequence of pictures we can see that the small structures are moving fast, while the large structures slowly (see fig.: 5.21). Important consequence of this is that the time scale of the flow is relatively small where the small structures occur and much more larger where the big structures are found. Thus, in the decaying region, especially in the side of the shear layer zone where larger structures can be found, the Reynolds averaged quantities need long averaging time (T_a) to converge. In the decaying region the curves from the simulation data hold some uncertainty, probably because of the insufficient convergence of the statistics. However in the developing region, where the small fast structures can be found the time statistics seems to be well converged.

λ_2 criteria

The vorticity is a measure of the rotation of a fluid element as it moves in the flow field, and is defined as the curl of the velocity vector:

$$\omega = \nabla \times u$$

This coherent structure detecting method is based on the inviscid Navier-Stokes equation (Euler equation). λ_2 is the second largest eigenvector of the $S_{ik}S_{kj} + \Omega_{ik}\Omega_{kj}$ tensor. Negative λ_2 values can be detected in the vortices. It can be seen that structures which are strongly rotating (big Q or small λ_2 value) can only be found near to the gas gun exit. The structures mostly align in the azimuthal direction when they appear at the gas gun exit, but they are broken quickly in downstream direction (triggered by the inlet turbulence) and the vorticity of the structures turn into downstream direction. Structures with both positive and negative streamwise vorticity can be found.

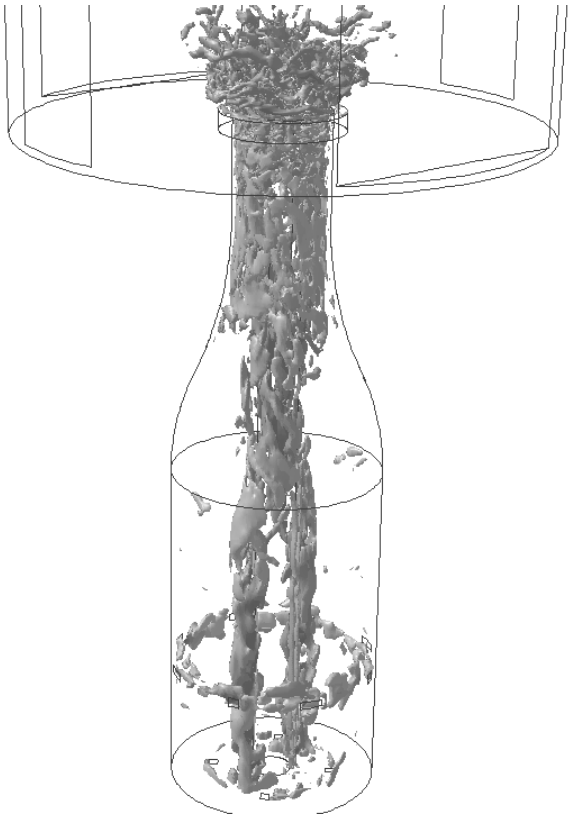

Figure 5.14: λ_2 isosurface with streamwise vorticity

Detecting the pressure minimum

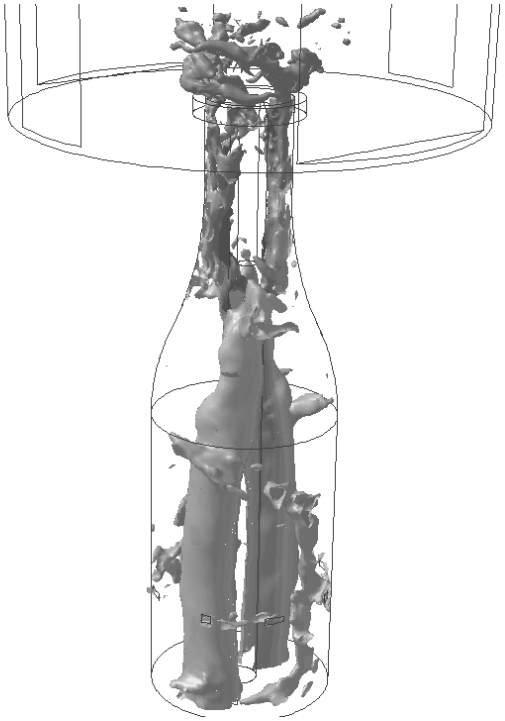

Figure 5.15: Isosurfaces of the fluctuating pressure $\overline{p'}$

Besides Q and λ_2 criteria, rotating structures can be detected according to the local pressure minimum criteria. This is obvious if we consider the inviscid Navier-Stokes equation in the natural coordinate system. For the efficient structure detecting, not the absolute pressure but the fluctuating pressure (defined as $\overline{p'} = \overline{p} - \langle\overline{p}\rangle$) was used. The isosurface can be seen in fig 5.24. These structures are more continuous than Q or λ_2. We can see more or less coherent vortex ring next to the inflow, and big structures further downstream. Thus the $\overline{p'}$ isosurfaces represent well the coherent structures resulting from the shear layer instability at the inflow, but at the same time they cannot show the same structure downstream.

Chapter 6

Conclusion

Large eddy simulations of turbulent swirling flows in a lab-scale swirl combustor are carried out for different configurations with two different swirl numbers to investigate the flow and turbulence structures, to validate the LES method and to examine the influence of boundary conditions, combustor geometry and turbulence structure.

Both the time-averaged mean velocity components and the variances of velocity fluctuations obtained from LES are found to be in good agreement with the corresponding experimental data. With a sufficient grid resolution and suitable inflow and outflow boundary conditions, LES successfully predicted the experimentally measured mean velocity and the variances. The LES and the experimental data reveal several important features of the confined swirling flow in the swirl combustor configuration.

The outflow conditions affect the results mostly at downstream region near the outlet; however at very high swirl numbers the effect of the outflow condition can be evident in the whole flow field. The onset of vortex breakdown is not very sensitive to the combustor length and the outlet configuration, but very sensitive to the sudden expansion at the inlet. The inflow swirl generator is found to be influential on the size and position of the internal recirculation zone.

The confined swirling flow fields in swirl combustor can be divided into different zones. Along the radial direction, a core zone near the axis, a shear layer near the edge of the sudden expansion. Vortex breakdown occurs when the swirl number is high enough. The fast decay of turbulence in confined swirling flows is due to the fast transport of turbulent kinetic energy in the radial direction, as a result of the high centrifugal force induced by the swirling motion. The enhanced turbulent kinetic energy transported to the wall is dissipated effectively by the viscous layer near the outer wall. This mechanism can successfully explain the low decay rate of turbulence in swirling jet flows.

Bibliography

[1] S. Abdallah: *Comments on the fractional step method*. J. Comput. Phys. Vol. 117 pp. 179-180, 1995

[2] N.A. Adams, S. Stolz: *A Subgrid-Scale Deconvolution Approach for Shock Capturing*. J. Comput. Phys. Vol. 178 pp. 391-426, 2002

[3] AGARD: *A Selection of Test Cases for the Validation of Large-Eddy Simulations of Turbulent Flows*. ADVISORY REPORT 345, NATO, 1998

[4] A. Aprovitola, F.M. Denaro: *On the application of congruent upwind discretizations for large eddy simulations*. J. Comput. Phys. Vol. 194 pp. 329-343, 2004

[5] R. Aris: Vectors, *Tensors and the Basic Equations of Fluid Mechanics*. Dover, 1989

[6] S. Armfield, R. Street: *The Fractional-Step Method for the Navier-Stokes Equations on Staggered Grids: The Accuracy of Three Variations*. J. Comput. Phys. Vol. 153 pp. 660-665, 1999

[7] I. Babuska, J.T. Oden: *Verification and validation in computational engineering and science: basic concepts*. Comput. Methods Appl. Mech. Engrg. Vol. 193 pp. 4057-4066, 2004

[8] J.S. Baggett, J. Jiménez, A.H. Kravchenko: *Resolution requirements in large-eddy simulations of shear flows*. Annual Research Briefs - Center for Turbulence Research, pp. 51-66, 1997

[9] J. Bardina, J.H. Ferziger, W.C. Reynolds: *Improved turbulence models based on large eddy simulation of homogeneous, incompressible, turbulent flows*. Report TF-19, Thermosciences Division, Dept. Mechanical Engineering, Stanford University, 1983

[10] T.J. Barth, P.O. Frederickson: *Higher Order Solution of the Euler Equations on Unstructured Grids Using Quadratic Reconstruction*. AIAA Paper 90-0013, 1990

[11] J.B. Bell, P. Colella, H.M. Glaz: *A Second-Order Projection Method for the Incompressible NavierStokes Equations*. J. Comput. Phys. Vol. 85 pp. 257-283, 1989

[12] S. Benhamadouche, K. Mahesh, G. Constantinescu: *Colocated finite-volume schemes for large-eddy simulation on unstructured meshes*. Proceedings of the Summer Program - Center for Turbulence Research, pp. 143-154, 2002

[13] L.C. Berselli, T. Iliescu, W.J. Layton: *Mathematics of Large Eddy Simulation of Turbulent Flows*. Springer, 2005

[14] L.C. Berselli, V. John: Asymptotic behaviour of commutation errors and the divergence of the Reynolds stress tensor near the wall in the turbulent channel flow. Math. Meth. Appl. Sci. Vol. 29 pp. 1709-1719, 2006

[15] L.C. Berselli, C.R. Grisanti, V. John: Analysis of commutation errors for functions with low regularity. Jou. Comput. App. Math. Vol. 206 pp. 1027-1045, 2007

[16] C. Bogey, C. Bailly: On the application of explicit spatial filtering to the variables or fluxes of linear equations. J. Comput. Phys. Vol. 225 pp. 1211-1217, 2007

[17] S.T. Bose, P. Moin, D. You: Grid-independent large-eddy simulation using explicit filtering. Annual

Research Briefs - Center for Turbulence Research, pp. 173-187, 2008

[18] F.F. Grinstein, L.G. Margolin, W.J. Rider: Implicit Large Eddy Simulation. Cambridge University Press, 2007

[19] T. Brandt: Usability of explicit filtering in large eddy simulation with a low-order numerical scheme and different subgrid-scale models. Int. J. Num. Meth. Fluids Vol. 57 pp. 905-928, 2008

[20] D.L. Brown, R.Cortez, M.L. Minion: Accurate Projection Methods for the Incompressible NavierStokes Equations. J. Comput. Phys. Vol. 168 pp. 464-499, 2001

[21] W. Cabot: Large-eddy simulations with wall models. Annual Research Briefs - Center for Turbulence Research, pp. 41-50, 1995

[22] W. Cabot, J. Jiménez, J.S. Baggett: On wakes and near-wall behavior in coarse large-eddy simulation of channel flow with wall models and second-order finite-difference methods. Annual Research Briefs - Center for Turbulence Research, pp. 343-354, 1999

[23] F. Capizzano, G. Iaccarino: Synthetic jet modeling for U-RANS. Proceedings of the Summer Program Center for Turbulence Research, pp. 183-194, 2004

[24] D. Carati, K. Jansen, T. Lund: A family of dynamic models for large-eddy simulation. Annual Research Briefs - Center for Turbulence Research, pp. 35-40, 1995

[25] D. Carati, E. Vanden Eijnden: On the self-similarity assumption in dynamic models for large eddy simulations. Phys. Fluids Vol. 9 No. 7, 1997

[26] D. Carati, A.A. Wray: Time filtering in large eddy simulations. Proceedings of the Summer Program Center for Turbulence Research, pp. 263-270, 2000

[27] D. Carati, G.S. Winckelmans, H. Jeanmart: On the modelling of the subgrid-scale and filtered-scale stress tensors in large-eddy simulation. J. Fluid Mech. Vol. 441 pp. 119-138, 2001

[28] FLUENT 6.3: User's Guide. Fluent Inc., 2006

[29] R.D. Moser, J. Kim, N. Mansour: Direct numerical simulation of turbulent channel flow up to Re_{τ}=590. Phys. Fluids Vol. 11 No. 4 pp. 943-945, 1999

[30] H. Choi, P. Moin: Effects of the computational time step on the numerical solutions of the

turbulent flow. J. Comput. Phys. Vol. 114 pp. 1-4, 1994

[31] A.J. Chorin: A numerical method for solving incompressible viscous flow problems. J. Comput. Phys. Vol. 2 pp. 12-26, 1967

[32] A.J. Chorin: Numerical solution of the Navier-Stokes equations. Math. Comput. Vol. 22 pp.745-762, 1968

[33] A.J. Chorin: On the convergence of discrete approximations to the Navier-Stokes equations. Math. Comput. Vol. 23 pp. 341-353, 1969

[34] A.J. Chorin, J.E. Marsden: A Mathematical Introduction to Fluid Mechanics. Springer, 3rd Ed'93

[35] F. Chow, P. Moin: A further study of numerical errors in large eddy simulation. J. Comput. Phys. Vol. 184 pp. 366-380, 2003

[36] F. Chow, R.L. Street, M. Xue, J.H. Ferziger: Explicit filtering and Reconstruction Turbulence Modeling for Large-Eddy Simulation of Neutral Boundary Layer Flow. Jou. Atm. Sci. Vol. 62 pp. 2058-2077, 2005 [37] J. Dandois, E. Garnier, P. Sagaut: Unsteady Simulation of a Synthetic Jet in a Crossflow. AIAA Jou. Vol. 44 No. 2 pp. 225-238, 2006

[38] M.S. Darwish: A New High-Resolution Scheme Based on the Normalized Variable Formulation. Num. Heat. Transf. Vol. 24 No. 3 pp. 353-371, 1993

[39] L. Davidson: LESFOIL: A European Project on Large Eddy Simulations Around a High-Lift Airfoil at High Reynolds Number. ECCOMAS 2000, Barcelona

[40] U. Piomelli: High Reynolds number calculations using the dynamic subgrid-scale stress model. Phys. Fluids A Vol. 5 No. 6 pp. 1484-1490, 1993

[41] G. De Stefano, O. Vasilyev: Sharp cutoff versus smooth filtering in large eddy simulation. Phys. Fluids Vol. 14 No. 1 pp.362-369, 2002

[42] S.B. Pope: Turbulent Flows. Cambridge University Press, 2003

[43] W. Deardorff: A numerical study of three-dimensional turbulent channel flow at large Reynolds numbers. J. Fluid Mech. Vol. 41 pp. 453-480, 1970

[44] O. Debliquy, B. Knaepen, D. Carati, A.A. Wray: Sampling versus filtering in Large-Eddy simulations. Proceedings of the Summer Program - Center for Turbulence Research, pp. 133-144, 2004

[45] J.C. Del Álamo, J. Jiménez, P. Zandonade, R.D. Moser: Scaling of the energy spectra of turbulent channels. J. Fluid Mech. Vol. 500 pp. 135-144, 2004

[46] F.M. Denaro: On the application of the Helmholtz-Hodge decomposition in projection methods for incompressible flows with general boundary conditions. Int. J. Num. Meth. Fluids Vol. 43 pp. 43-69, 2003 [47] F.M. Denaro: Time-accurate intermediate boundary conditions for large eddy simulations based on projection methods. Int. J. Num. Meth. Fluids Vol. 48 pp. 869-908, 2005

[48] C. Fureby, F.F. Grinstein: Large Eddy Simulation of High-Reynolds-Number Free and Wall-Bounded Flows. J. Comput. Phys. Vol. 181 pp. 68-97, 2002

[49] F. Sarghini, U. Piomelli, E. Balaras: Scale-similar models for large-eddy simulations. Phys. Fluids Vol. 11 No. 6 pp. 1596-1607, 1999

[50] D. Drikakis, W. Rider: High-Resolution Methods for Incompressible and Low-Speed Flows. Springer, 2005

[51] U. Schumann: Subgrid scale model for finite difference simulations of turbulent flows in plane channels and annuli. J. Comput. Phys. Vol. 18 pp. 376-404, 1975

[52] C. Wagner, T. Hüttl, P. Sagaut: Large-Eddy Simulation for Acoustics. Cambridge University Press, 2007

[53] P. Sagaut: Large Eddy Simulation for Incompressible Flows. Springer, 3rd Ed, 2006

[54] R.J. LeVeque: Finite Volume Methods for Hyperbolic Problems. Cambridge University Press, 2006

[55] J. Gullbrand, F. Chow: The effect of numerical errors and turbulence models in large-eddy simulations of channel flows, with and without explicit filtering. J. Fluid Mech. Vol. 495 pp. 323-341, 2003

[56] S. Hoyas, J. Jiménez: Scaling of the velocity fluctuations in turbulent channels up to Re_τ=2003. Phys. Fluids Vol. 18 No. 1, 2006

[57] C. Fureby, F.F. Grinstein: Monotonically Integrated Large Eddy Simulation of Free Shear Flows. AIAA Jou. Vol. 37 No. 5, 1999

[58] E. Garnier, N. Adams, P. Sagaut: Large Eddy Simulation for Compressible Flows. Springer, 2009

[59] P.H. Gaskell, A.K.C. Lau: Curvature-compensated convective transport: SMART a new boundednesspreserving transport algorithm. Int. J. Num. Meth. Fluids Vol. 8 pp. 617-641, 1988

[60] M. Germano, U. Piomelli, P. Moin, W. Cabot: A dynamic subgrid-scale eddy viscosity model. Phys. Fluids A Vol. 3 No. 7 pp.1760-1765, 1991

[61] M. Germano: Turbulence: the filtering approach. J. Fluid Mech. Vol. 238 pp. 325-336, 1992

[62] S. Ghosal: On the large eddy simulation of turbulent flows in complex geometry. Annual Research Briefs - Center for Turbulence Research, pp. 111-128, 1993

[63] S. Ghosal: Analysis of the discretization errors in LES. Annual Research Briefs - Center for Turbulence Research, pp. 3-24, 1995

[64] Hunt, J. C. R., Wray, A. A. and Moin, P., *Eddies, stream, and convergence zones in turbulent flows*, Center for Turbulence Research Report, CTR-S88 (1988), 193-208